

THE USE OF HIGH RESOLUTION HEIGHT DATA IN THE COMPUTATION OF
HIGH PRECISION GEOID HEIGHTS ON THE ISLAND OF MAUI

A Thesis

Presented in Partial Fulfillment of the Requirements for the degree
Master of Science in the Graduate School of the Ohio State
University

by
Dru A. Smith, B.S.

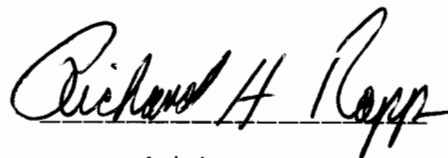
The Ohio State University
1991

Master's Examination Committee:

Dr. Richard Rapp

Dr. Clyde Goad

Approved by

A handwritten signature in black ink, reading "Richard H. Rapp". The signature is written in a cursive style with a horizontal line underneath the name.

Adviser,

Department of Geodetic
Science and Surveying

To my parents
Darlene F. Ray
The Late Dean A. Smith

ACKNOWLEDGMENTS

I am very grateful to the various people who helped me throughout this process, both directly and indirectly. I am especially grateful to my advisor, Dr. Richard H. Rapp, who kept my motivation for this project high, despite numerous computational difficulties. I am also grateful to the number of graduate researchers who were old hands at the computer system at Ohio State, and were willing to take time out of their schedules to answer my unending questions, especially Nikos Pavlis and Chein-Way Hwang.

A great deal of thanks to Nancy Kaler for her help in getting this monster typed. Word processing and Geodesy don't mix very well.

I am also very grateful to my family and friends who supported me both directly and indirectly from beginning to end.

VITA

September 22, 1967 Born - Toledo, Ohio
1989 B.S., The Ohio State University
Columbus, Ohio

FIELDS OF STUDY

Major Field: Geodetic Science and Surveying

TABLE OF CONTENTS

TITLE PAGE	i
DEDICATION	ii
ACKNOWLEDGMENTS	iii
VITA	iv
TABLE OF CONTENTS	v
LIST OF TABLES	vii
LIST OF FIGURES	ix
 1. INTRODUCTION	 1
2. FORMULAS USED	3
2.1 The Stokes' Integral	3
2.2 Assumptions in the Stokes' Integral	4
2.3 Potential Coefficient Models	5
2.4 Truncation Theory	7
3. GRAVITY REDUCTIONS AND EXTERNAL MASSES	11
3.1 Free-Air Reduction	11
3.2 External Masses	14
3.3 Indirect Effect and Secondary Indirect Effect	16
3.4 Atmospheric Corrections	19
4. PHYSICAL DATA NEAR THE LASER STATION	21
4.1 The Laser Station	21
4.2 Geometric Data	26
4.3 Gravimetric Data	30
4.4 Elevation Data	35
5. COMPUTATIONAL METHODS AND NUMERICAL RESULTS	37
5.1 Computational Methods	37
5.1.1 The Sensitivity of the Geoid Undulation to Numerical Integration of the Stokes' Integral	 37
5.1.1.1 The Integration Point	38
5.1.1.2 The Use of Sub-Cells	40
5.1.1.3 Interpolation vs. Calculation of the Stokes' function	 41
5.1.1.4 Eight ways to integrate numerically the Stokes' Integral	 46
5.2 Numerical Results	49

5.2.1. Computational Variables.....	49
5.2.2 Terrain Correction Calculations.....	51
5.2.2.1 The Crustal Density.....	68
5.2.3 Local Average Correction.....	72
5.2.4 The Cap Calculations.....	77
5.2.5 The Outer Zone Calculations.....	84
5.2.5.1 Ellipsoidal Corrections.....	85
5.2.6 Undulation from Various Potential Coefficient Models.....	86
5.2.7 The Entire Geoid Undulation.....	88
5.2.8 Discussion of Results.....	94
6. SUMMARY AND CONCLUSIONS.....	98
6.1 Summary of Results.....	98
6.2 Conclusions.....	100
6.3 Areas of Future Research.....	101
REFERENCES.....	103

LIST OF TABLES

TABLE	PAGE
1. Geometric parameters of four reference ellipsoids	26
2. Coordinates of 7120 and 7210 on 1987 ellipsoid from SL6 reference system and on 1991 ellipsoid from SL7.1 reference system	30
3. Geometric and gravimetric parameters of two reference ellipsoids	31
4. Normal gravity values at the pole and equator on two ellipsoids	32
5. Comparison of linearly interpolating and rigorously calculating the Stokes' function, ψ in seconds	43-44
6. Statistical values of terrain corrections over land areas (mgal), $\rho=2.67 \times 10^3$ kg/m ³	64
7. Statistical values of terrain corrections over sea areas (mgal), $\rho=2.67 \times 10^3$ kg/m ³	64
8. Terrestrial and PCM mean anomalies and their respective local average corrections	75
9. Cap contribution from free-air gravity anomalies using $\Delta\sigma$ breakdown of Despotakis (64-16-4-1 sub-cells)	79

10.	Cap contribution from free-air gravity anomalies using new $\Delta\sigma$ breakdown (1600 sub-cells)	80
11.	Terrain correction contributions to the geoid undulation cap calculation (N_{TC})	81
12.	Cap contribution to the geoid undulation, in meters, $\rho=2.67 \times 10^3 \text{ kg/m}^3$	82
13.	Cap contribution to the geoid undulation, in meters, $\rho=2.9 \times 10^3 \text{ kg/m}^3$	83
14.	Outer zone contribution (meters) to the geoid undulation	84
15.	Ellipsoidal corrections using various reference fields. Units are meters	85
16.	Outer zone contribution (meters) to the geoid undulation plus ellipsoidal corrections. Units are meters	86
17.	Geoid undulations calculated by reference fields alone. Units are meters	88
18.	Geoid undulation from the Combined Cap, Outer Zone, Indirect Effect, and Ellipsoidal Corrections, Old system	90
19.	Geoid undulation from the Combined Cap, Outer Zone, Indirect Effect, and Ellipsoidal Corrections, New system	91
20.	Given undulations minus calculated undulations, Old system. Units are cm	92
21.	Given undulations minus calculated undulations, New system. Units are cm	93
22.	Undulation calculations from Despotakis (ibid)	96

LIST OF FIGURES

FIGURE	PAGE
1. The relationship between the ellipsoid, geoid, and Earth's surface	12
2. The location of masses before condensation	16
3. The location of masses, and co-geoid after condensation	17
4. 3-D view of 5'x5' mean bathymetric and MSL elevations near Maui. View is from Southwest, at an elevation of 30 degrees, looking Northeast	23
5. 3-D view of 5'x5' mean elevations above Mean Sea Level near Maui. View is from Southwest, at an elevation of 30 degrees, looking Northeast	24
6. Contour map of 5'x5' elevations above Mean Sea Level. C.I. = 200 m	25
7. Distribution of point free-air gravity anomalies from NGS and L-D GOCU	33
8. 1991 Free-air gravity anomaly contours with C.I. = 25 mgal	34
9. Location of land, cap and 3" elevations inside a 5 degree area	36

10.	An example of a properly referenced $\Delta\sigma$ cell yielding correct ψ	39
11.	An example of an improperly referenced $\Delta\sigma$ cell yielding incorrect ψ	39
12.	Difference between linearly interpolating and rigorously calculating the Stokes' function relative to ψ	45
13.	Division of $5^\circ \times 5^\circ$ area into 4 parts for $30'' \times 30''$ TC calculation, (method #1)	56
14.	3" Terrain corrections, using $20' \times 20'$ FFT with 5' border, C.I.=2 mgal, Area surrounding Mt. Mauna Kea (Code number 2.12)	57
15.	3" Terrain corrections, using $10' \times 10'$ FFT with 10' border, C.I.=2 mgal, Area surrounding Mt. Mauna Kea (Code number 2.12)	58
16.	3" Terrain corrections, using $20' \times 20'$ FFT with 5' border, C.I.=2 mgal, Area surrounding Mt. Haleakala	59
17.	3" Terrain corrections, using $10' \times 10'$ FFT with 10' border, C.I.=2 mgal, Area surrounding Mt. Haleakala	60
18.	Locations and code numbers of $20' \times 20'$ areas where 1600 sub-cells were used and $3'' \times 3''$ terrain corrections were calculated	61
19.	Elevation plot around Mauna Kea using 3" elevations, C.I.=100 m (Code number 2.12)	65
20.	Elevation plot around Mauna Kea using $30''$ elevations, C.I.=100 m (Code number 2.12)	66
21.	Terrain correction plot around Mauna Kea using $30''$ TC's, C.I.=2 mgal (Code number 2.12)	67

CHAPTER I

INTRODUCTION

The purpose of this study is to determine various effects on precise geoid undulation computations at two laser tracking stations located on Mt. Haleakala, Maui, Hawaii. The emphasis of this study is on the effect of precise terrain corrections on geoid undulations, but other effects were also studied.

The original computations upon which this study were based were from a thesis done by Despotakis (1987). The gravity data, used both in this report and by Despotakis, were two minute by two minute mean free-air gravity anomalies, derived from point free-air anomalies and altimetry in a five degree by five degree area surrounding the two laser stations.

Numerous computational changes were made, and their effects upon the geoid undulation were studied. This study will include the effect of different methods of terrain correction computation; different potential coefficient reference fields and maximum degrees of expansion; different ellipsoidal parameters and different crustal densities assumed for terrain correction computations.

Many computational methods were used throughout this study, some of which have been used unquestioningly for years due to their relative accuracy. Now with the accuracy of ellipsoidal parameters

and geoid undulations approaching centimeter level, these set techniques are seen to reveal errors which were, in the past, considered negligible. There is, however, a trade-off for not using the old assumptions -- computer time. Often the use of approximations can save many minutes of computer time which will only yield changes on the centimeter level. It is now necessary to re-evaluate the approximations made in geoid computations based on accuracy requirements for the final geoid undulation.

Chapter 2 explains the formulas used in the computation of the geoid undulation. In particular, truncation theory is discussed.

Chapter 3 deals with the necessary gravity reductions and corrections necessary for the formulas in Chapter 2 to be valid.

Chapter 4 describes the physical locations and attributes of the laser stations. The different geodetic reference systems are also discussed in this chapter.

Chapter 5 outlines the various methods of numerically integrating the Stokes' integral and their effects on the undulation. It also contains the final undulations obtained using the different computational schemes; different geodetic reference systems; different crustal densities; and different potential reference fields and maximum degrees of expansion.

Chapter 6 summarizes the computations done in this study and draws conclusions from those computations. Also, possible future sources of research are mentioned.

CHAPTER II

FORMULAS USED

2.1 The Stokes' Integral

The Stokes' integral is one of the fundamental formulas in physical geodesy, and was first used by G.G. Stokes in 1849 to solve for geoid undulations from terrestrial anomalies (Heiskanen and Moritz, 1967):

$$N = \frac{R}{4\pi\gamma} \iint_{\sigma} \Delta g S(\psi) d\sigma \quad (2-1)$$

where:

R	mean earth radius
γ	mean normal gravity for the earth
σ	the sphere of integration
$S(\psi)$	Stokes' function
Δg	gravity anomaly, to be discussed in Chapter 3

For a clear derivation of the Stokes' integral see Zhao (1989). The development of the Stokes' integral is not relevant here, only the

knowledge that many approximations are made for equation 2-1 to be valid when applied to the earth.

2.2 Assumptions in the Stokes' Integral

Most gravimetric computations are initially formulated with many assumptions, with corrections made to the initial result to give more correct results. This is done because formulas are less complex when selected assumptions are made. This section will deal with the derivation of the most correct geoid computations starting from first assumptions.

The Stokes' integral is extremely simple in its formulation, but very unrealistic assumptions are made for it to work, to the accuracy required, in its original form. They are (Despotakis, *ibid*):

- 1) The surface of the geoid is a sphere
- 2) Integration is carried out over the entire geoid with an infinite number of point gravity anomalies
- 3) No mass outside of the geoid exists (both terrestrial and extra-terrestrial)
- 4) The mass of the reference ellipsoid is equal to the true mass of the earth
- 5) The normal potential on the ellipsoid equals the gravity potential on the geoid
- 6) The ellipsoid's center coincides with the earth's center of mass.

Some of these assumptions or approximations require the calculation of correction terms that will yield more accurate results. For example, the spherical approximation (item 1) may be removed by applying ellipsoidal correction terms which are discussed in Section 5.2.5.1. Also, the integration over the entire geoid (item 2) may be replaced with a computational method known as Molodensky's truncation method which is discussed in Section 2.4. The existence of external masses can be removed using Helmert's second method of condensation which is discussed in Chapter 3.

2.3 Potential Coefficient Models

The classical method of solving Laplace's equation has been through the use of spherical harmonics, using an infinite series of fully normalized potential coefficients (FNPC's), \bar{C}_{nm} and \bar{S}_{nm} :

$$V(r, \theta, \lambda) = \frac{GM}{r} \sum_{n=0}^{\infty} \left(\frac{a}{r} \right)^n \sum_{m=0}^n \left(\bar{C}_{nm} \cos m\lambda + \bar{S}_{nm} \sin m\lambda \right) \bar{P}_{nm}(\cos \theta) \quad (2-2)$$

where:

$V(r, \theta, \lambda)$	Potential at a point $P(r, \theta, \lambda)$
r	Geocentric distance to point P
θ	Co-latitude of point P
λ	Longitude of point P
GM	Geocentric gravitational constant of the earth

a	Equatorial radius of ellipsoid which refers r, θ, λ
\bar{P}_{nm}	Fully normalized Legendre functions
n	Degree
m	Order, $m \leq n$

The term potential coefficient model (PCM) will refer to any group of FNPC's known up to some degree. Despotakis (ibid) used the PCM OSU86F (Rapp and Cruz, 1986) - a PCM complete to degree 360. He used it only up to degree 180 in his computations. In addition to OSU86F, the more recent models OSU89B and OSU91A will be used in this study. The numerical results from different PCM's are tabulated in Chapter 5.

In areas of the world where the geoid changes gradually, an accurate PCM up to degree 180 or 360 may yield acceptable results in the calculation of the undulation. In areas of rugged terrain, such as Hawaii, where the geoid changes rapidly, errors of meters can occur if the PCM alone is used to calculate the undulation, because high frequency information cannot be obtained considering the degree to which current PCM's are known. Therefore, the PCM is best used in combination with terrestrial gravity data for the computation of the undulation. This combination is known as truncation theory and is discussed in the next section.

2.4 Truncation Theory

The idea of integrating over the entire geoid with an infinite number of gravity anomalies is a limiting factor in geoid computations for two reasons. The first is the inability to ever have an infinite number of gravity anomalies, and the second is the decreasing effect which gravity anomalies have on the geoid as one goes further away from a small area around a point of interest. The area surrounding a point of interest is called a "cap" while the area outside of the cap is called the "outer zone". The idea of truncation theory is the summing of two influences on the geoid undulation, one from the cap and one from the outer zone, to get the whole undulation. The computation of the cap contribution will be done with terrestrial gravity data, while the outer zone effect is computed using a high degree potential coefficient model. The computation of these two individual influences is simpler than attempting an integration over the entire geoid.

It is important to note that neither the cap contribution nor the outer zone contribution will be errorless, even if no errors enter into the collection of their individual data. The cap will never have an infinite number of gravity anomalies and the outer zone will never have an infinite number of potential coefficients. However, dense gravity anomalies and high degree reference fields may give results to the accuracy needed for the determination of the geoid.

Truncation theory is based upon changing the way the Stokes' integral is evaluated. First, the integration is broken into two

parts, one for the surface of the geoid inside the cap (σ_c) and one for the outer zone ($\sigma - \sigma_c$):

$$N = \frac{R}{4\pi\gamma} \iint_{\sigma_c} \Delta g S(\psi) d\sigma + \frac{R}{4\pi\gamma} \iint_{\sigma - \sigma_c} \Delta g S(\psi) d\sigma \quad (2-3)$$

The following derivation is from Despotakis (ibid).

The first half of equation (2-3) is the final version of the cap contribution, however, the outer zone effect needs to be derived from the second half of equation (2-3). This part, if integrated over the whole sphere, could be changed in to a Legendre series. Therefore, we introduce a new function:

$$\bar{S}(\psi) = \begin{cases} 0 & 0 \leq \psi \leq \psi_c \\ S(\psi) & \psi_c < \psi \leq \pi \end{cases} \quad (2-4)$$

So that:

$$\frac{R}{4\pi\gamma} \iint_{\sigma - \sigma_c} \Delta g S(\psi) d\sigma = \frac{R}{4\pi\gamma} \iint_{\sigma} \Delta g \bar{S}(\psi) d\sigma \quad (2-5)$$

Expanding:

$$\bar{S}(\psi) = \sum_{n=0}^{\infty} \frac{2n+1}{2} Q_n(\psi_c) P_n(\cos \psi) \quad (2-6)$$

where:

$Q_n(\psi_c)$ the Fourier coefficients of \bar{S}

Since $2\pi Q_n(\psi_c)$ are the eigenvalues of the integral operator of the right-hand side of equation (2-5), equation (2-5) gives:

$$\frac{R}{4\pi\gamma} \iint_{\sigma-\sigma_c} \Delta g S(\psi) d\sigma = \frac{R}{2\gamma} \sum_{n=0}^{\infty} Q_n(\psi_c) \Delta g_n \quad (2-7)$$

Substituting into equation (2-3) yields:

$$N = \frac{R}{4\pi\gamma} \iint_{\sigma_c} \Delta g S(\psi) d\sigma + \frac{R}{2\gamma} \sum_{n=0}^{\infty} Q_n(\psi_c) \Delta g_n \quad (2-8)$$

where:

$$\Delta g_n(r, \theta, \lambda) = \frac{GM}{r^2} (n-1) \left(\frac{a}{r} \right)^n \sum_{m=0}^n \left(\bar{C}_{nm} \cos m\lambda + \bar{S}_{nm} \sin m\lambda \right) \bar{P}_{nm}(\cos \theta) \quad (2-9)$$

$\bar{C}_{nm}, \bar{S}_{nm}$ Fully normalized Potential Coefficients
of the Disturbing Potential

a the equatorial radius of the ellipsoid used in
the computation of the FNPC's.

For a complete derivation, see Despotakis (ibid, pp 6-10)

From the preceding equations, we can see that the two effects on the geoid undulation, cap and outer zone, come from the

terrestrial anomalies and the spherical harmonic reference field, respectively. Both will have errors, since the numerical integration only approximates the true cap integration and the spherical harmonic reference field is only known up to a finite degree.

CHAPTER III

GRAVITY REDUCTIONS AND EXTERNAL MASSES

3.1 Free-Air Reduction

The gravity anomaly used in the Stokes' integral is the difference between gravity on the geoid (g_P) and normal gravity on the ellipsoid (γ_Q):

$$\Delta g = g_P - \gamma_Q \quad (3-1)$$

Normal gravity may be calculated using equation (3-2):

$$\gamma = \frac{a \gamma_a \cos^2 \phi + b \gamma_b \sin^2 \phi}{\sqrt{a^2 \cos^2 \phi + b^2 \sin^2 \phi}} \quad (3-2)$$

where:

γ_a	normal gravity at the equator
γ_b	normal gravity at the pole
a	semi-major axis of ellipsoid
b	semi-minor axis of ellipsoid

Gravity is not measured on the geoid itself, but on the surface of the earth (see figure 1). Let g_S be the measured value, g_P be the reduced value on the geoid, and H be the orthometric height between points P and S .

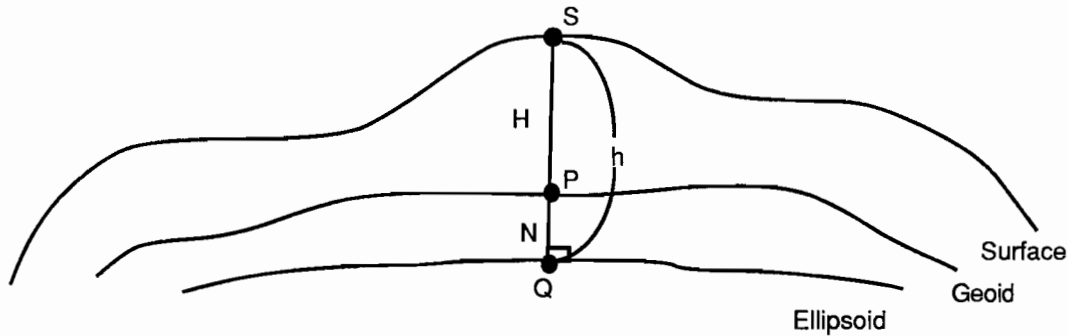


FIGURE 1

The relationship between the Ellipsoid, Geoid, and Earth's Surface

If we assume that no masses exist between the geoid and the surface of the earth, then equation (3-3) shows the mathematical connection between g_P and g_S :

$$g_P = g_S - \frac{\partial g}{\partial H} H - \frac{1}{2} \frac{\partial^2 g}{\partial H^2} H^2 - \dots \quad (3-3)$$

For simplicity, we assume gravity changes linearly over H , so that (3-3) becomes:

$$g_P \approx g_S - \frac{\partial g}{\partial H} H \quad (3-4)$$

Since we don't know $\partial g / \partial H$ we estimate it by $\partial \gamma / \partial h$ so that:

$$g_P \approx g_S - \frac{\partial \gamma}{\partial h} H \quad (3-5)$$

The value $-(\partial \gamma / \partial h)H$ is known as the free-air gradient (F), and has the value:

$$F = (.3086) H \quad (3-6)$$

Thus:

$$g_P \approx g_S + F = g_S + (.3086)H \quad (3-7)$$

Through equations (3-1), (3-2) and (3-7), we are able to calculate Δg values at any point (ϕ, λ) , given ϕ, λ, g_S, H . These free-air anomalies may be used in the Stokes' integral for the calculation of the geoid undulation. However, the undulation calculated using free-air anomalies will not be the correct undulation because masses external to the geoid exist, which contradicts our earlier assumption. The next sections will discuss how to correct the 'free-air undulation' by mathematically shifting the external masses so they are no longer external to the geoid.

3.2 External Masses

The undulation obtained using free-air gravity anomalies in the Stokes' integral contains errors because Laplace's equation is not satisfied rigorously. Therefore, some mathematical scheme must be used to shift or move the masses so that they are no longer external to the geoid. This shifting of the external masses may change both the free-air gravity anomalies and the location of the geoid itself. This second change, known as the indirect effect, can be very complicated to compute, depending on the method used to shift the external masses (Wichiencharoen, 1982). Therefore, it is desirable to choose a method of shifting the external masses which has a small, easy to calculate, indirect effect. The indirect effect will be discussed in more detail in section 3.3.

Helmert's second method of condensation will be the method used in this study to shift the external masses because of its simple formulation and small indirect effect. Helmert's second method of condensation does not remove the external masses, but condenses them down along the local vertical to form an infinitesimally thin layer of mass on the geoid, so that the total mass of the earth remains unchanged. This reduces, but does not eliminate the indirect effect.

Schematically, Helmert's second method of condensation may be thought of as removing all external masses and then condensing them back in an infinitesimally thin layer on the geoid. Heiskanen and Moritz (1967, p. 145) claim that the removal of the topography

compensates that of the condensed layer and therefore: 'the free-air anomalies may be considered as approximations of condensed anomalies.' As will be seen later, this is not true to today's accuracy. Moritz (1968, p. 41) states that the difference between the attraction of the external masses and the condensed layer is the terrain correction, which is, in a flat-earth approximation:

$$TC_P = \frac{1}{2} G \int_{-\infty}^{+\infty} \int_{-\infty}^{+\infty} \frac{\rho(x,y) [h(x,y) - h_p]^2}{d^3} dx dy \quad (3-8)$$

where:

- (x_P, y_P) point where TC is calculated
- (x, y) each point distant from (x_P, y_P) , used in the calculation of TC
- h_P height of point $P(x_P, y_P)$
- $h(x, y)$ height of point (x, y)
- $d = \sqrt{(x - x_P)^2 + (y - y_P)^2}$
- $\rho(x, y)$ crustal density of mass-column at (x, y)

The Helmert anomalies are:

$$\Delta g_H = \Delta g + TC \quad (3-9)$$

The formulation of the terrain corrections approximates the curved earth by a flat plane extending to infinity. The errors introduced due

to this approximation will be assumed negligible for the purposes of this study.

3.3 Indirect Effect and Secondary Indirect Effect

The condensation of the masses external to the geoid causes a gravitational potential change everywhere. Thus, when the masses are shifted (condensed, removed, etc.) the equipotential surface originally associated with the true geoid moves to a new position and is now called the co-geoid. See Figures 2 and 3.

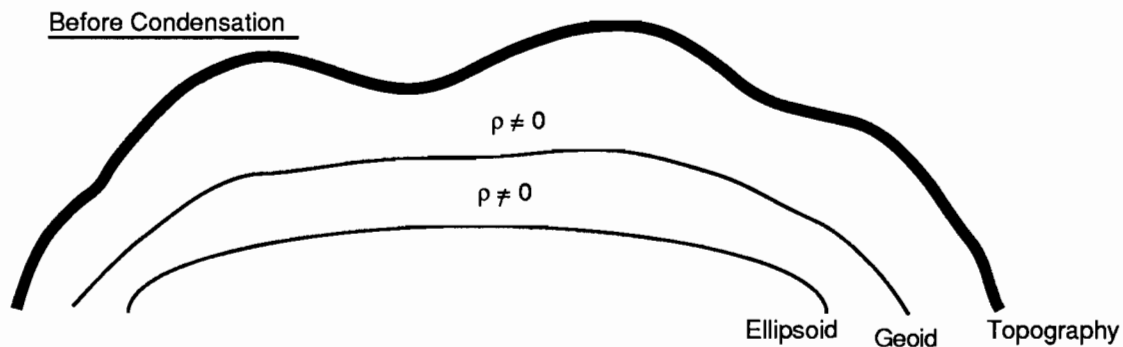


FIGURE 2

The location of masses before condensation

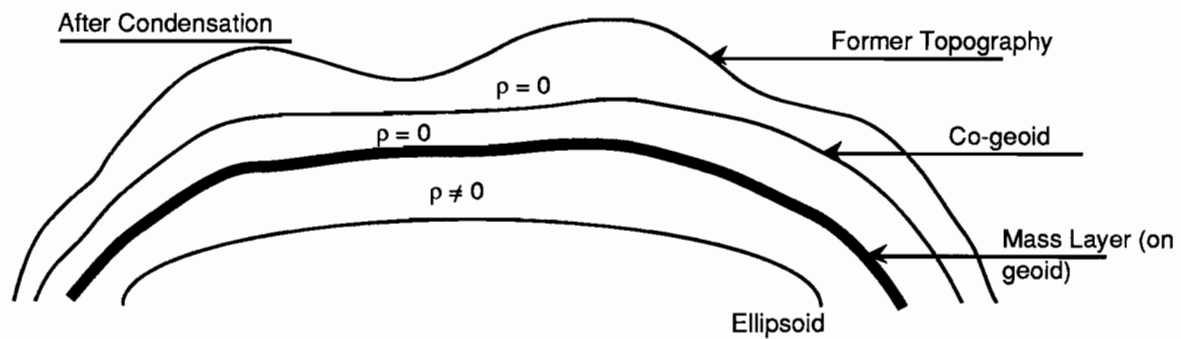


FIGURE 3

The location of masses, and co-geoid after condensation

The difference in elevation between the geoid and the co-geoid (δN_I) at a point is known as the indirect effect on the geoid undulation and can be computed knowing the change in potential (δW), caused by the condensing of the masses, through Brun's formula:

$$\delta N_I = \frac{\delta W}{\gamma} \quad (3-10)$$

Wichiencharoen (ibid) investigated many ways to calculate the indirect effect and found that the simplest way, though less accurate, was using Grushinsky's formula:

$$\delta N_I = \frac{-\pi G \rho H^2}{\gamma} \quad (3-11)$$

This will be the formula used in this study for the calculation of the indirect effect. Through equation (3-11) we see that the indirect effect is always negative. This means that in Helmert's second method of condensation, the co-geoid lies above the geoid.

It is very important to note that the use of the Helmert anomalies in the Stokes' integral will yield the undulations of the co-geoid, not the geoid. This is because the location of the equipotential surface associated with the modified geoid is computed. Therefore, the indirect effect must be added to the Helmert undulation to get the undulation of the undisturbed, or original geoid:

$$N = \frac{R}{4\pi\gamma} \iint_{\sigma_c} \Delta g_H S(\psi) d\sigma + \frac{R}{2\gamma} \sum_{n=0}^{\infty} Q_n(\psi_c) \Delta g_n + \delta N_I \quad (3-12)$$

However, this formula is not yet complete. As stated, the co-geoid undulation is calculated using the Helmert anomalies. But the Helmert anomalies refer to the geoid, not the co-geoid, and so they must be corrected to refer to the co-geoid if the undulation of the co-geoid is to be correctly calculated. Because the co-geoid lies above the geoid, and no masses exist between the two surfaces, a free-air reduction is done to reduce the Helmert anomalies from the geoid to the co-geoid. This free-air reduction is known as the secondary indirect effect on the gravity anomalies (δg_{SI}):

$$\delta g_{SI} = .3086 \delta N_I \quad (3-13)$$

Thus, δg_{SI} is added to Δg_H in Stokes' integral to yield the undulation of the co-geoid, and δN_I is added to that to yield the undulation of the geoid:

$$N = \frac{R}{4\pi\gamma} \iint_{\sigma_c} (\Delta g_H + \delta g_{SI}) S(\psi) d\sigma + \frac{R}{2\gamma} \sum_{n=0}^{\infty} Q_n(\psi_c) \Delta g_n + \delta N_I \quad (3-14)$$

3.4 Atmospheric Corrections

One more external mass will be considered in this study -- the mass of the atmosphere. Like Helmert's second method of condensation, the mass of the atmosphere is condensed down along the local vertical to the geoid. Therefore, a correction to the Helmert anomalies must be computed as well as the indirect effect and secondary indirect effect of condensing the atmosphere. However, the indirect effect on geoid undulations and secondary indirect effect on gravity anomalies due to condensing the atmosphere are considered negligible, so we shall only calculate corrections to the Helmert anomalies. This is one of the most difficult corrections to calculate precisely due to the constantly shifting masses and changing atmospheric densities. Yet it is also very small (under 1 mgal) and so if a reasonably accurate model of the atmosphere is used, the correction can be calculated to the accuracy needed. One such model is (Wichiencharoen, *ibid*):

$$\delta g_A = \left(0.8658 - 9.727 \times 10^{-5} H + 3.482 \times 10^{-9} H^2 \right) \text{mgals} \quad (3-15)$$

where:

H orthometric height in meters

These corrections are added to the Helmert anomalies and used in the Stokes' integral:

$$N = \frac{R}{4\pi\gamma} \iint_{\sigma_c} (\Delta g_H + \delta g_{SI} + \delta g_A) S(\psi) d\sigma + \frac{R}{2\gamma} \sum_{n=0}^{\infty} Q_n(\psi_c) \Delta g_n + \delta N_I \quad (3-16)$$

CHAPTER IV

PHYSICAL DATA NEAR THE LASER STATION

4.1 The Laser Station

The laser tracking station of interest in this study is on Mt. Haleakala, the highest peak on the island of Maui. Two benchmarks are located at this station, points 7120 and 7210. Point 7120 is a physical monument, but 7210 is defined as the intersection of the horizontal and vertical antennae axes of the laser mount.

Figure 4 shows a three dimensional view of 5'x5' mean elevations in the 5 degree area surrounding the laser station ($18^{\circ} \leq \phi \leq 23^{\circ}$, $201^{\circ} \leq \lambda \leq 206^{\circ}$). Most of these elevations are bathymetric, with only the smallest tip of each high point being an island. However, the quick rise of these masses from the sea floor causes the islands to be very steep and rugged, meaning that terrain corrections will need to be calculated on as small of a grid as possible. Figure 5 shows the same elevations, with bathymetry removed, that is only the masses above the sea level are shown. Due to the nature of the plotting package used, the vertical scale is highly exaggerated, yet it is useful to see that certain islands (Hawaii, especially) rise much higher and steeper than some surrounding islands.

In Figures 4 and 5, the longitude is the azimuth of the viewer, relative to the figure, from south, positive east and the latitude is the angle of elevation of the viewer. Thus in Figure 4, the viewer is Southwest of the islands (-45°), elevated 30 degrees above sea level, looking Northeast toward the islands.

Initial plots made of this area indicated that the 80,000 point shoreline file used for the contour maps, in subroutine World of the GSPP plotting package, contained variable errors. Upon checking the shoreline file with USGS quad sheets, the errors in the shoreline file were found to be:

$$5' < \text{error}_\phi < 13'$$

$$-7' < \text{error}_\lambda < 2'$$

Because no systematic shift was found between the shoreline file, and values measured from USGS quad sheets, two options were available -- 1) apply a different correction to each point in the shoreline file to properly align it with USGS values or 2) apply a systematic shift which would give a 'best fit' visually between the zero elevation line (from the 5' elevation data) and the shoreline. In the interest of time, option 2 was used. The best fit between the zero elevation line and the shorelines was found by adding the following shifts to the shoreline points in the 5 degree area of interest:

$$\phi_{\text{new}} = \phi_{\text{old}} + 12' 2''$$

$$\lambda_{\text{new}} = \lambda_{\text{old}} - 6' 53''$$

An elevation contour map with these shifts is shown in Figure 6.

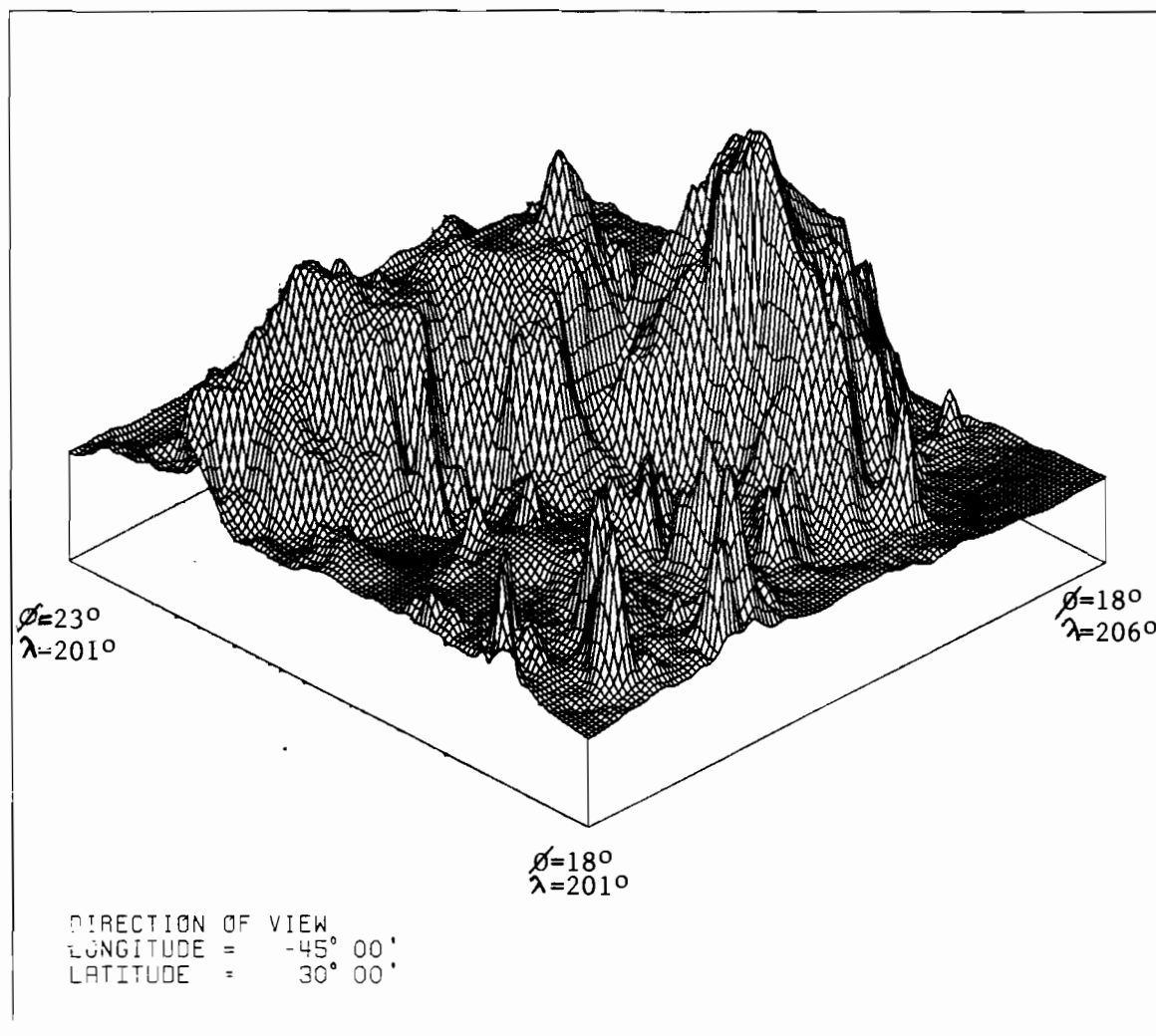


FIGURE 4

3-D view of 5'x5' mean bathymetric and MSL elevations near Maui.

View is from Southwest, at an elevation of 30 degrees, looking
Northeast

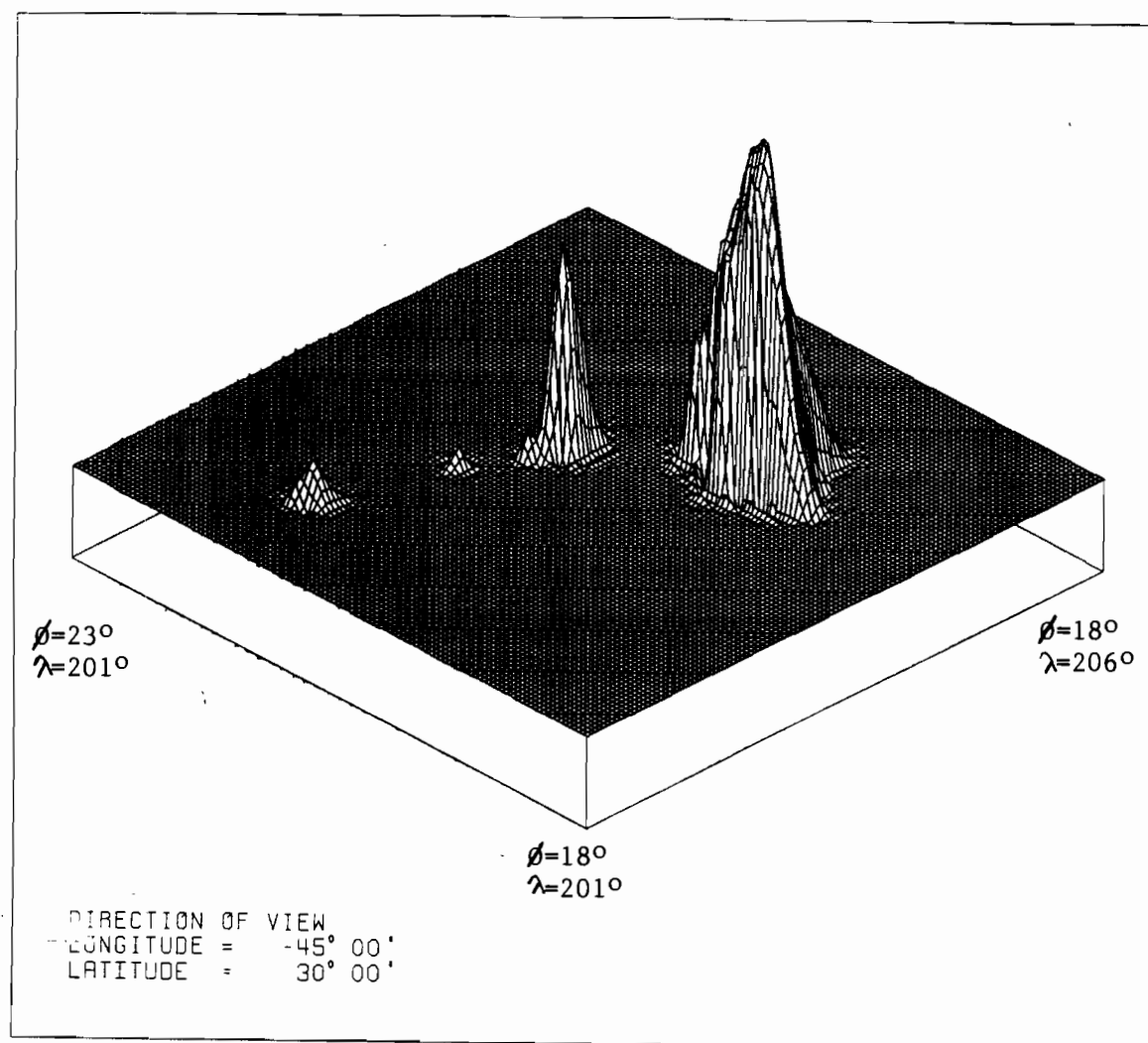


FIGURE 5

3-D view of 5'x5' mean elevations above Mean Sea Level near Maui.

View is from Southwest, at an elevation of 30 degrees, looking
Northeast

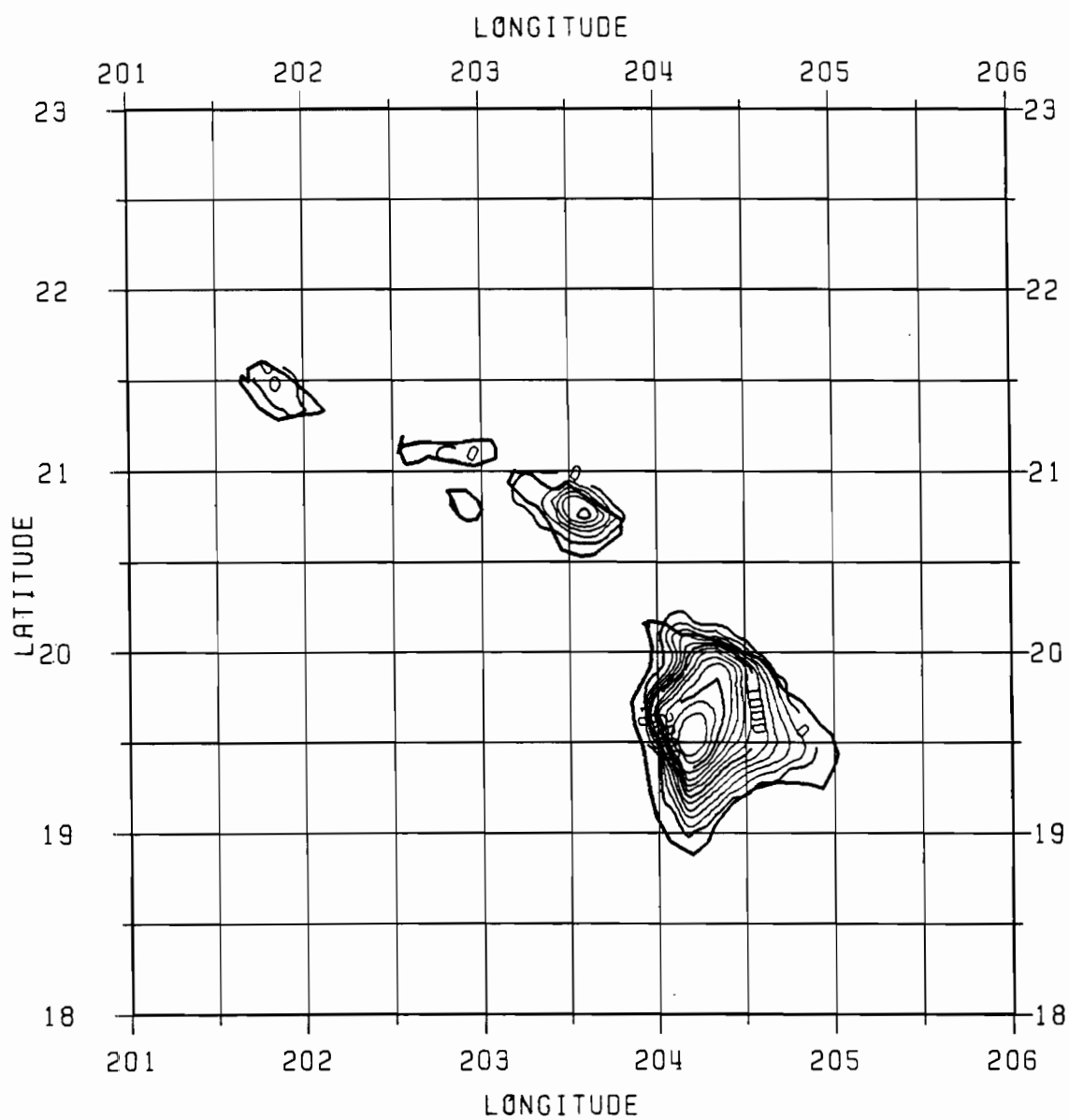


FIGURE 6

Contour map of 5'x5' elevations above Mean Sea Level. C.I.=200 m

4.2 Geometric Data

The original geodetic coordinates of the laser stations were given in the SL6 system (Robbins, 1985), which were converted to the OSU GRS reference ellipsoid of 1987 (Despotakis, 1987). More recent coordinates were given for these stations in the SL7.1 system (Pavlis, 1991), which were then converted to the OSU GRS reference ellipsoid of 1991. The geometric parameters of these four ellipsoids are given below:

TABLE 1
Geometric parameters of four reference ellipsoids

Ellipsoid	a (meters)	1 / f
SL 6	6378144.11	298.255
OSU GRS 87	6378136.0	298.257222101
SL 7.1	6378137.0	298.257
OSU GRS 91	6378136.3	298.257222101

The equatorial radius of OSU GRS 91 is from Rapp (1991).

The following methods were used for transforming geodetic coordinates from one reference ellipsoid to another (Goad, 1988):

$$(\phi, \lambda, h)_{\text{SL 6}} \rightarrow (x, y, z) \rightarrow (\phi, \lambda, h)_{\text{OSU GRS 87}}$$

$$(\phi, \lambda, h)_{\text{SL 7.1}} \rightarrow (x, y, z) \rightarrow (\phi, \lambda, h)_{\text{OSU GRS 91}}$$

The first step in these transformations makes use of the following equations:

$$\begin{aligned} X &= (N + h) \cos \phi \cos \lambda \\ Y &= (N + h) \cos \phi \sin \lambda \\ Z &= (N(1-e^2) + h) \sin \phi \end{aligned} \quad (4-1)$$

where:

N radius of curvature in the prime vertical
e first eccentricity of the ellipsoid

The second step uses an iterative process around ϕ and h , as well as the following equation:

$$\lambda = \tan^{-1} (Y/X) \quad (4-2)$$

The iterative process (Goad, 1988) is based on the following relation between changes in the Cartesian quantities P (horizontal distance from spin axis) and Z (vertical distance above equatorial plane) and changes in the geodetic quantities ϕ and h :

$$\begin{bmatrix} \Delta P \\ \Delta Z \end{bmatrix} = \begin{bmatrix} \frac{\partial P}{\partial \phi} & \frac{\partial P}{\partial h} \\ \frac{\partial Z}{\partial \phi} & \frac{\partial Z}{\partial h} \end{bmatrix} \begin{bmatrix} \Delta \phi \\ \Delta h \end{bmatrix} \quad (4-3)$$

where:

$$P = (N + h) \cos \phi \quad (4-4)$$

$$Z = (N(1-e^2) + h) \sin \phi \quad (4-5)$$

Equation (4-3) may alternately be written:

$$\begin{bmatrix} \Delta\phi \\ \Delta h \end{bmatrix} = \begin{bmatrix} \frac{\partial P}{\partial \phi} & \frac{\partial P}{\partial h} \\ \frac{\partial Z}{\partial \phi} & \frac{\partial Z}{\partial h} \end{bmatrix}^{-1} \begin{bmatrix} \Delta P \\ \Delta Z \end{bmatrix} \quad (4-6)$$

Step 1) Given X, Y, Z, calculate true P and Z:

$$P = \sqrt{X^2 + Y^2} \quad (4-7)$$

$$Z = Z \quad (4-8)$$

Step 2) Use P and Z to calculate approximate values of ϕ and h:

$$\phi = \tan^{-1} (Z/P) \quad (4-9)$$

$$h = \sqrt{P^2 + Z^2} - 6371000 \text{ (meters)} \quad (4-10)$$

Step 3) Calculate N:

$$N = \frac{a}{\sqrt{1 - e^2 \sin^2 \phi}} \quad (4-11)$$

Step 4) Calculate P and Z from the approximate values of ϕ and h:

$$P = (N + h) \cos \phi$$

$$Z = (N(1 - e^2) + h) \sin \phi$$

Step 5) Calculate ΔP , ΔZ , $\partial P/\partial \phi$, $\partial P/\partial h$, $\partial Z/\partial \phi$, $\partial Z/\partial h$ and use equation 4-4 to get $\Delta \phi$ and Δh . If $\Delta \phi$ and Δh are less than a set tolerance (10^{-10} radians for ϕ , and 10^{-10} m for h) then the iteration stops. Otherwise, add $\Delta \phi$ and Δh to old values of ϕ and h and repeat steps 3-5.

The orthometric heights used by Despotakis (1987) were given originally by Alfano (1986) but more recent values became available from Pavlis (1991). These different values are given in Table 2. The orthometric heights are given with respect to an unclearly defined reference mean sea level which cause some uncertainties in the N values.

As a basis for comparison, two sets of different geodetic coordinates and different orthometric heights were used throughout this study -- 1) Old values (from SL.6) referring to OSU GRS 87 and 2) Newer values (from SL.7.1) referring to OSU GRS 91.

The coordinates of the two stations are shown in Table 2.

TABLE 2

Coordinates of 7120 and 7210 on 1987 ellipsoid from SL6 reference system and on 1991 ellipsoid from SL7.1 reference system.

STA.	ELLIPSOID	SYSTEM	ϕ	λ	h (m)	H (m)	N=h - H
7120	OSU GRS 87	SL.6	20° 42' 27.3880"	203° 44' 38.1020"	3068.7162	3048.2530	20.4632
7210	OSU GRS 87	SL.6	20° 42' 25.9920"	203° 44' 38.6000"	3069.2871	3048.7980	20.4891
7120	OSU GRS 91	SL7.1	20° 42' 27.3946"	203° 44' 38.2422"	3068.4885	3048.2529	20.2356
7210	OSU GRS 91	SL7.1	20° 42' 25.9761"	203° 44' 38.7427"	3068.2231	3047.9500	20.2731

4.3 Gravimetric Data

The free-air gravity anomalies used by Despotakis (1987) were derived from point values from the National Geodetic Survey (NGS) and the Lamont-Doherty Geological Observatory of Columbia University (L-D GOCU) as well as altimetry data. Where point values had insufficient coverage, altimetry values were used to assign values to the blank areas. The distribution of the point values is shown in Figure 7. The final result was a 5°×5° free-air gravity anomaly file with 2'×2' mean values in the area $18^{\circ} \leq \phi \leq 23^{\circ}$, $201^{\circ} \leq \lambda \leq 206^{\circ}$.

The free-air gravity anomalies used by Despotakis (ibid) refer to OSU GRS 87. These were transformed to refer to OSU GRS 91 for

this study. The geometric and gravimetric constants used in this transformation are given in Table 3:

TABLE 3
Geometric and gravimetric parameters of two reference ellipsoids

Ellipsoid	a (meters)	1 / f	GM (km ³ /s ²)	ω (rad/s)
OSU GRS 87	6378136.0	298.257222101	398600.440	7.29115x10 ⁻¹¹
OSU GRS 91	6378136.3	298.257222101	398600.436	7.29115x10 ⁻¹¹

The new value of GM is that used in GEM-T2 (Marsh, 1989).

The transformation scheme used is similar to that used by Despotakis (ibid), where:

$$\Delta g_{87} = g_{\text{obs}} - \gamma_{87} + .3086 H \quad (\text{mgal, meter}) \quad (4-12)$$

and

$$\Delta g_{91} = g_{\text{obs}} - \gamma_{91} + .3086 H \quad (\text{mgal, meter}) \quad (4-13)$$

where:

H is Orthometric Height.

Since g_{obs} and $.3086 H$ are the same in both systems, the following relation can be written:

$$\Delta g_{91} = \Delta g_{87} + \gamma_{87} - \gamma_{91} \quad (4-14)$$

Table 4 shows the normal gravity values for both systems at the equator and pole.

TABLE 4

Normal gravity values at the pole and equator on two ellipsoids

Ellipsoid	γ_a (mgal)	γ_b (mgal)
OSU GRS 87	983,125.0830	979,828.8507
OSU GRS 91	983,124.9807	979,828.7487

These values are then used with equation (3-2) to find the value $\gamma_{87} - \gamma_{91}$:

$$\gamma_{87} - \gamma_{91} = 0.102 \text{ mgal} \quad (4-15)$$

Thus, 0.102 mgal must be added to the 1987 free-air gravity anomalies to refer them to the 1991 ellipsoid constants.

A contour map of the point anomalies in the 1991 system of constants, with a contour interval of 25 mgal, is shown in Figure 8. The maximum and minimum values of the free-air gravity anomalies are 675.234 and -133.943 mgals respectively.

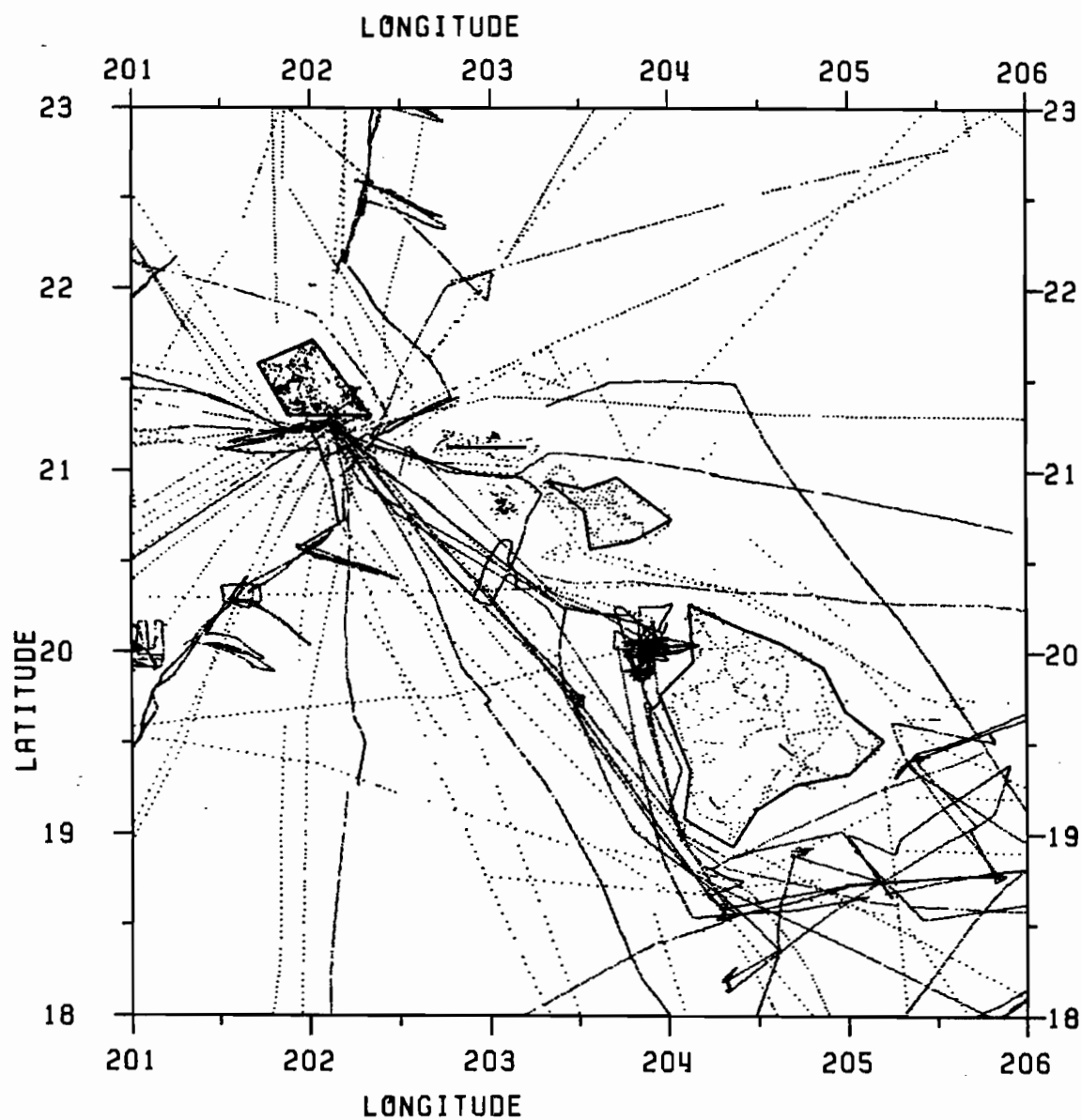


FIGURE 7

Distribution of point free-air gravity anomalies from NGS and
L-D GOCU

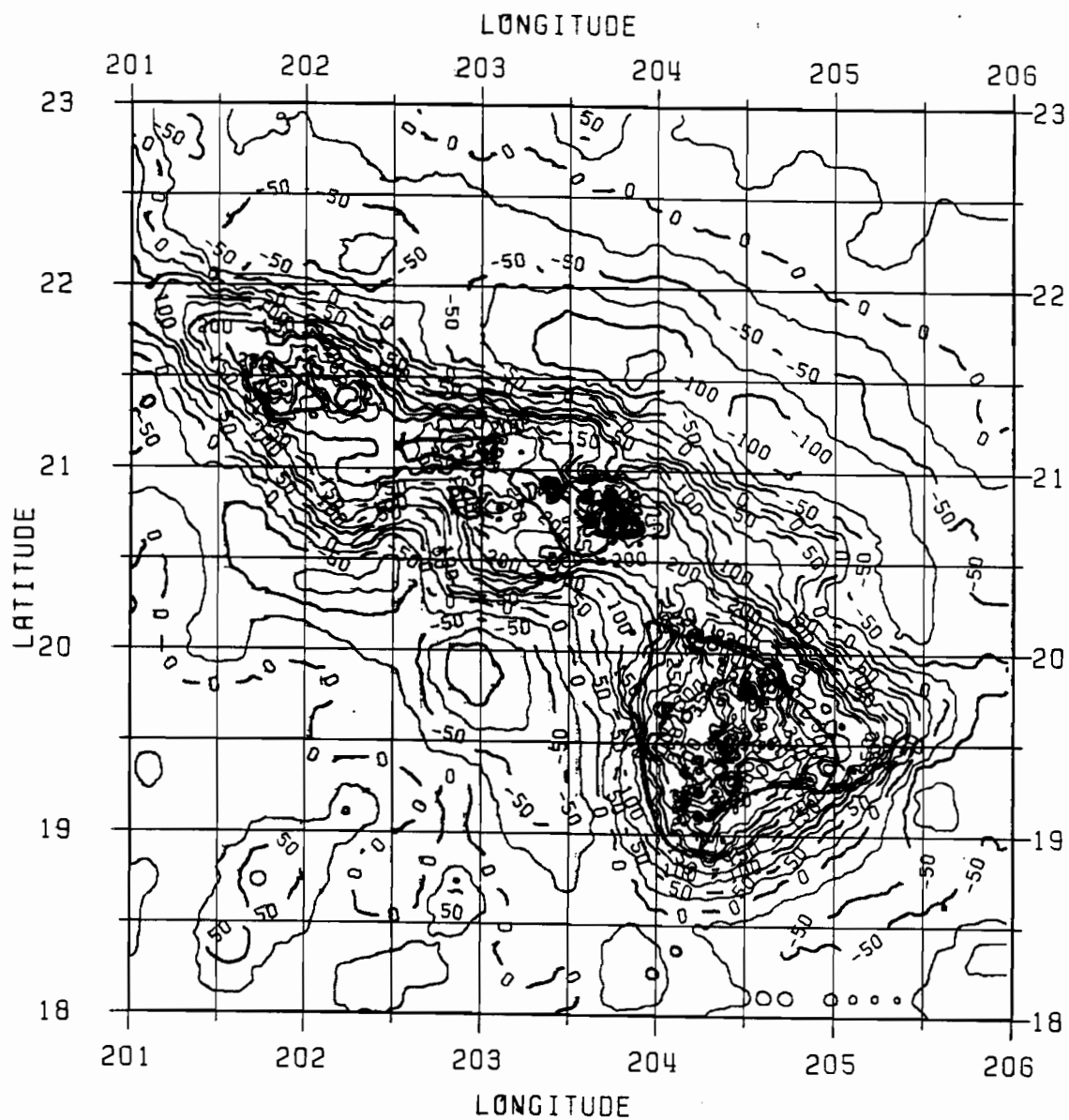


FIGURE 8

1991 Free-air gravity anomaly contours with C.I.= 25 mgal

4.4 Elevation Data

Two sources of elevation data were available -- 5'x5' gridded mean elevations to 1 meter, which we will call ETOPO5U (Sloss, 1988) and 3"x3" gridded point elevations to 1 meter which we will call DMA DTED (U.S. Dept. of Defense, 1988). The 5' elevations were available globally, but the 3" elevations were only available in five 1°x1° cells near the laser station. Figure 9 shows where the 3" elevations were available.

As seen in Figure 9, most areas with land are covered by 3" elevations. In those areas with land, inside a cap of radius 2°, where 3" elevations were not available, the 5' values were densified into 3" values. This was done primarily so that numerical integration programs would have a consistent grid size with which to work. Due to the limited number of these areas and their distances from the laser station, the errors involved in this procedure will be considered negligible.

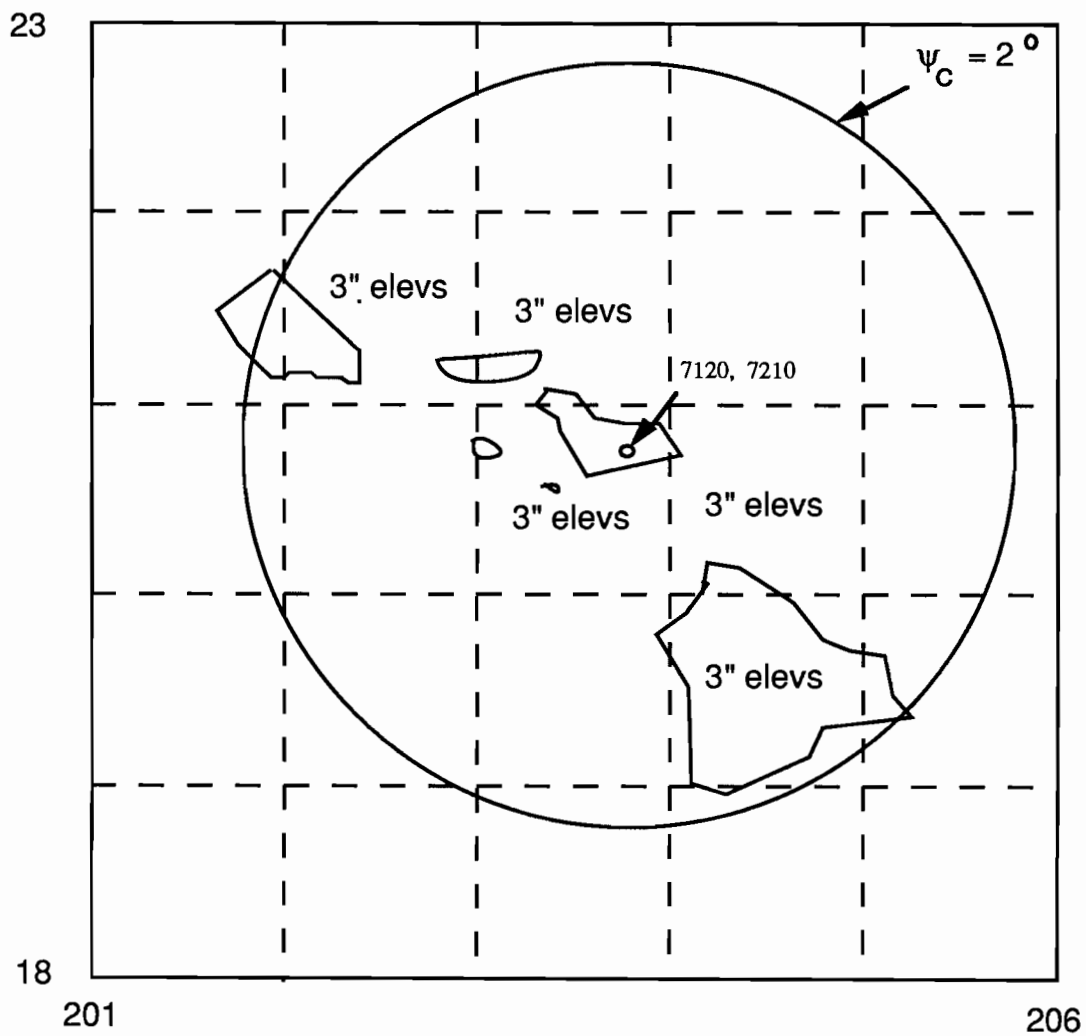


FIGURE 9

Location of land, cap and 3" elevations inside a 5 degree area

CHAPTER V

COMPUTATIONAL METHODS AND NUMERICAL RESULTS

5.1 Computational Methods

This section will explain the various computational methods used in this study. Many non-traditional computations were examined and used involving the numerical integration of the Stokes' Integral, and therefore will be explained in detail here.

5.1.1 The Sensitivity of the Geoid Undulation to Numerical Integration of the Stokes' Integral

This sub-section discusses the various ways that the geoid undulation computation can be affected by different interpretations of the numerical integration of the Stokes' Integral. The various ways of analytically treating the Stokes' Integral will be shown with conclusions drawn on which methods are more accurate than others, which are faster, and which are the overall best for use on a computer.

5.1.1.1. The Integration Point

Clearly, the integration of the Stokes' integral is not possible in an analytical sense, and therefore requires a numerical integration using finite cells, $\Delta\sigma$, in place of the infinitely small cells, $d\sigma$. This introduces the question of how to interpret the value of the spherical distance, ψ . The computationally simplest and crudest way is to compute a value of ψ to the center of each $\Delta\sigma$ cell (θ_c, λ_c) and do a numerical integration over the cap. The use of the center point of the $\Delta\sigma$ cell is important. To use any other point (θ, λ) to calculate ψ would mean the undulation obtained from equation (3-16) would refer to a point offset from the laser station by the same amount as the point (θ, λ) is offset from the (θ_c, λ_c) . See Figures 10 and 11 for details.

Improperly referenced $\Delta\sigma$ cells could introduce errors of a non-negligible size depending on the size of the $\Delta\sigma$ cell and how far the laser station (θ', λ') is from (θ_c, λ_c) . In Despotakis (ibid), each ψ was calculated to the Northwest corner, of each $\Delta\sigma$ cell, instead of the middle, which introduced errors in his cap contribution calculations on the order of 20 cm. It should be noted that the error was not introduced in his formulation of the problem, but in the computer program used to calculate the undulation. Thus, if formulas are not properly implemented, the results will not be correct.

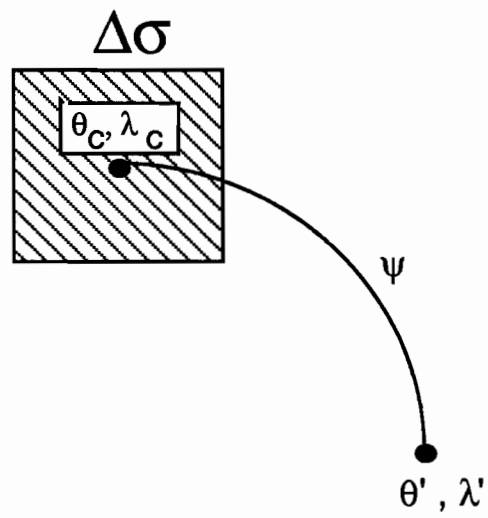


FIGURE 10

An example of a properly referenced $\Delta\sigma$ cell yielding correct ψ

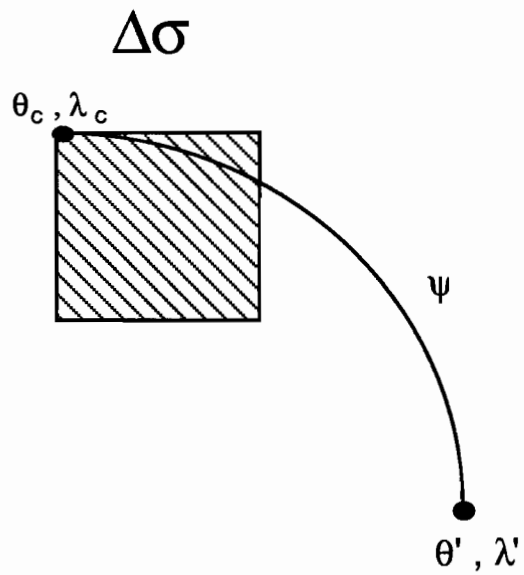


FIGURE 11

An example of an improperly referenced $\Delta\sigma$ cell yielding incorrect ψ

5.1.1.2 The Use of Sub-Cells

The idea of using sub-cells for more accurate numerical integration was adopted from Rapp (1975), with the changes made in Despotakis (ibid) to apply the sub-cell breakdown to a cap of radius 2° . The individual $\Delta\sigma$ cell (of size $2' \times 2'$) is broken down into sub-cells, the number depending upon ψ (calculated to the center of the original cell), which were then used in the numerical integration. Rapp (ibid) suggests the calculation of $S(\psi)$ for each ψ corresponding to a sub-cell. The average value of $S(\psi)$ is then used in the numerical integration of the entire cell. As will be seen in section 5.2.4, this method introduces noticeable but negligible errors (under 1cm) in the numerical integration procedure. The following method was initially used for the sub-cell breakdown:

$\psi \leq 4'$	64 sub-cells
$4' < \psi \leq 8'$	16 sub-cells
$8' < \psi \leq 12'$	4 sub-cells
$12' < \psi \leq 2^\circ$	1 sub-cell

where ψ refers to the spherical distance to the center of the original cell. This breakdown was modified when 3" elevation data was used so that the numerical integration of sub-cells would correspond exactly to the 3" elevation data (and thus 3" terrain corrections, atmospheric corrections and secondary indirect effects) which were available. Wherever 3" terrain corrections were calculated, the following scheme was used for sub-cell breakdown:

If 3" are data available, then divide 2'x2' $\Delta\sigma$ cell into 1600 sub-cells

The number of sub-cells (1600) corresponds exactly to the number of 3"x3" areas in one 2'x2' original cell. As will be seen, all cells where $\psi < 12'$ contain 3" data. Thus, when 3" data were used, the original breakdown scheme is voided, and the original $\Delta\sigma$ cells were either broken down into 1600 sub-cells (if 3" data was available) or 1 sub-cell (if no 3" data was available).

5.1.1.3 Interpolation vs. Calculation of the Stokes' function

One of the most time consuming functions of computing geoid undulations is the calculation of the Stokes' function at every point at which integration is carried out. Numerous people have chosen a simpler method of interpolating $S(\psi)$ from a table between full seconds of arc. This method is good while the accuracy of geoid computations remains greater than 1cm, but when the numerical integration is carried out in a very dense area surrounding the computation point, the interpolation may start to break down, and errors in geoid undulation computations may be noticeable at the 1 cm level. To check the possible errors in the interpolation of the Stokes' function, the calculated and interpolated values of $S(\psi)$ were compared. Table 5 shows that the error in the interpolation of $S(\psi)$ exceeds +1.0 when $\psi < 1'$, and gets increasingly worse as ψ approaches zero. This table is slightly deceiving, as maximum errors occur near

(but not exactly at) the half-second marks. As ψ approaches even seconds, the error $S_{\text{int}} - S_{\text{calc}}$ approaches zero. Figure 12 shows this phenomenon better.

TABLE 5

Comparison of linearly interpolating and rigorously calculating the
Stokes' function, ψ in seconds

ψ	S_{calc}	S_{int}	ΔS	ψ	S_{calc}	S_{int}	ΔS
0.5"	825096.1	412564.4	412,531.7	30.5"	13550.1	13553.7	3.6
1.5	275053.3	309431.0	34,377.6	31.5	13120.6	13123.9	3.3
2.5	165043.9	171919.4	6875.6	32.5	12717.6	12720.6	3.0
3.5	117896.6	120352.2	2455.6	33.5	12338.6	12341.3	2.7
4.5	91703.5	92849.5	1145.9	34.5	11981.5	11984.1	2.5
5.5	75035.1	75660.1	625.1	35.5	11644.6	11646.9	2.3
6.5	63495.3	63873.1	377.8	36.5	11326.2	11328.3	2.1
7.5	55032.7	55278.3	245.6	37.5	11024.7	11026.7	2.0
8.5	48561.3	48729.8	168.5	38.5	10738.9	10740.7	1.8
9.5	43452.2	43572.8	120.6	39.5	10467.5	10469.2	1.7
10.5	39316.3	39405.6	89.3	40.5	10209.6	10211.2	1.6
11.5	35899.6	35967.5	67.9	41.5	9964.1	9965.5	1.4
12.5	33029.6	33082.5	52.9	42.5	9730.1	9731.5	1.3
13.5	30584.7	30626.7	42.0	43.5	9506.9	9508.2	1.3
14.5	28477.1	28511.0	33.9	44.5	9293.7	9294.9	1.2
15.5	26641.4	26669.1	27.7	45.5	9089.9	9091.0	1.1
16.5	25028.2	25051.2	23.0	46.5	8894.9	8895.9	1.0
17.5	23599.3	23618.6	19.3	47.5	8708.0	8709.0	1.0
18.5	22324.9	22341.2	16.3	48.5	8528.9	8529.8	0.9
19.5	21181.2	21195.2	13.9	49.5	8357.0	8357.9	0.9
20.5	20149.1	20161.1	12.0	50.5	8191.9	8192.7	0.8

Table 5 (continued),

ψ	S_{calc}	S_{int}	ΔS	ψ	S_{calc}	S_{int}	ΔS
21.5"	19213.0	19223.4	10.4	51.5"	8033.2	8034.0	0.8
22.5	18360.1	18369.2	9.1	52.5	7880.6	7881.3	0.7
23.5	17579.8	17857.7	8.0	53.5	7733.6	7734.4	0.7
24.5	16863.1	16870.2	7.0	54.5	7592.1	7592.8	0.6
25.5	16202.7	16208.9	6.2	55.5	7455.7	7456.3	0.6
26.5	15592.1	15597.7	5.5	56.5	7324.1	7324.7	0.6
27.5	15025.9	15030.0	5.0	57.5	7197.1	7197.6	0.5
28.5	14499.5	14503.9	4.5	58.5	7074.4	7074.9	0.5
29.5	14008.7	14012.7	4.0	59.5	6955.8	6958.3	0.5
30.5	13550.1	13553.7	3.6	60.5	6841.1	6841.6	0.5

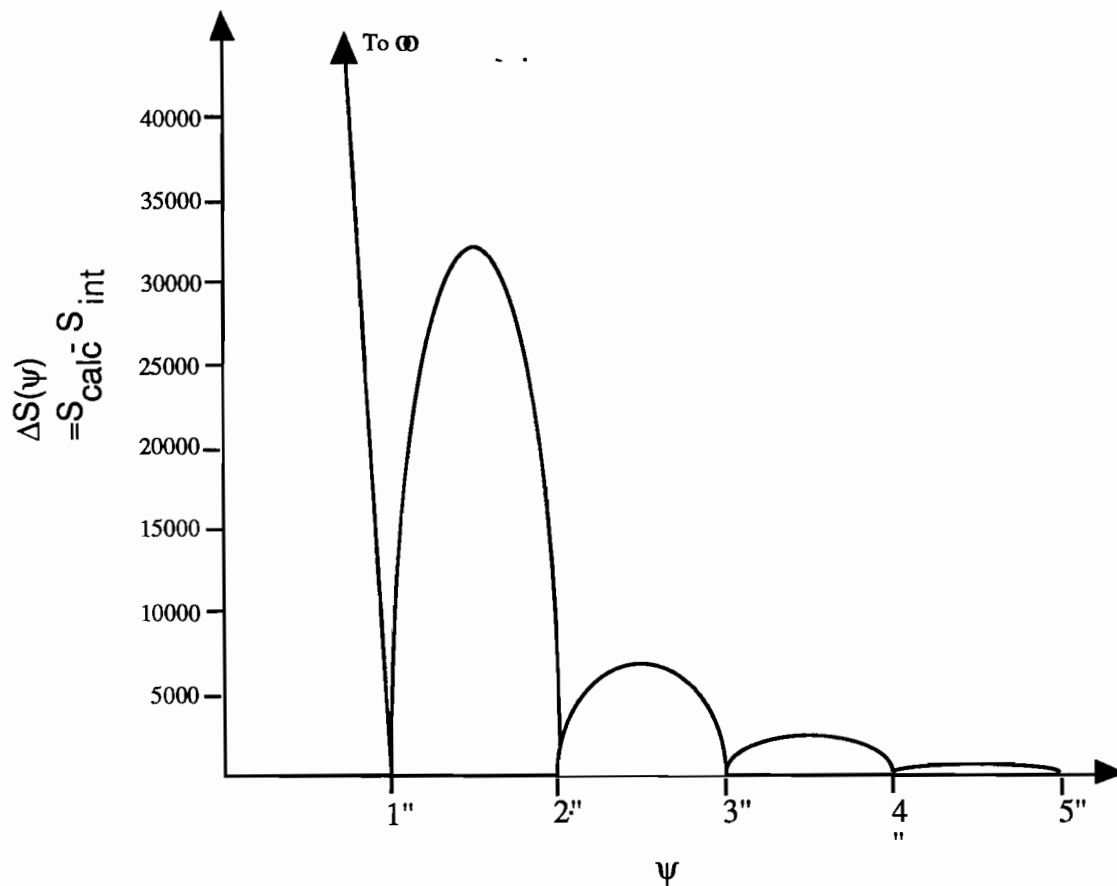


FIGURE 12

Difference between linearly interpolating and rigorously calculating the Stokes' function relative to ψ

If the sub-cell breakdown forces ψ to approach 30" or less, then the interpolated $S(\psi)$ value for a sub-cell will diverge from the true $S(\psi)$ value. Naturally, this will only occur in those cells directly surrounding the computation point, yet these are the most influential areas on the geoid undulation, and the possibility of this error affecting the geoid undulation should be considered. Therefore, due to the high number of sub-cells used around the laser

stations, calculation of the Stokes' function was chosen over interpolation for the sake of avoiding any possible errors which may be introduced. We will see in section 5.2.4 that the error introduced by interpolating the Stokes' function in this study is minimal (under 1 cm).

5.1.1.4 Eight ways to integrate numerically the Stokes' Integral

Written in a numerical integration form, the Stokes' integral is:

$$N = \frac{R}{4\pi\gamma} \sum_{\phi=18}^{23} \sum_{\lambda=201}^{206} \Delta g(\phi, \lambda) S[\psi(\phi, \lambda)] \Delta \sigma \quad (5-1)$$

where:

$$\psi(\phi, \lambda) \leq 2^\circ$$

$$\Delta \sigma = \Delta \phi \Delta \lambda = 2' \times 2' \text{ (in radians)}$$

$R, \pi, \gamma, \Delta g$ are all fixed for a certain ϕ, λ so the question is how to evaluate a particular $S[\psi(\phi, \lambda)] \Delta \sigma$ at each ϕ, λ . The following eight methods were investigated for their computational accuracy.

$$S(\psi) \Delta \sigma = \sum_{i=1}^n \sum_{j=1}^n S_{\text{calc}}(\psi_{ij}) \Delta \sigma_{ij} \quad (5-2a)$$

$$S(\psi)\Delta\sigma = \sum_{i=1}^n \sum_{j=1}^n S_{int}(\psi_{ij}) \Delta\sigma_{ij} \quad (5-2b)$$

$$S(\psi)\Delta\sigma = \frac{\sum_{i=1}^n \sum_{j=1}^n S_{calc}(\psi_{ij})}{n^2} \Delta\sigma \quad (5-3a)$$

$$S(\psi)\Delta\sigma = \frac{\sum_{i=1}^n \sum_{j=1}^n S_{int}(\psi_{ij})}{n^2} \Delta\sigma \quad (5-3b)$$

$$S(\psi)\Delta\sigma = S_{calc} \left(\frac{\sum_{i=1}^n \sum_{j=1}^n \psi_{ij}}{n^2} \right) \Delta\sigma \quad (5-4a)$$

$$S(\psi)\Delta\sigma = S_{int} \left(\frac{\sum_{i=1}^n \sum_{j=1}^n \psi_{ij}}{n^2} \right) \Delta\sigma \quad (5-4b)$$

$$S(\psi)\Delta\sigma = S_{calc}(\psi_{center}) \Delta\sigma \quad (5-5a)$$

$$S(\psi)\Delta\sigma = S_{int}(\psi_{center}) \Delta\sigma \quad (5-5b)$$

Note that the summations of i, j up to n refer to the sub-cell breakdown of the $\Delta\sigma$ cell. Equation 5-2a is the computationally longest method, yet it approaches true integration as n approaches infinity. Equation 5-3a uses an average value of $S(\psi)$, calculated from the individual $S(\psi)$ values corresponding to each sub-cell. Equation 5-4a uses an average value of ψ , calculated from the individual ψ values corresponding to each sub-cell, which is then used in the Stokes' function. Equation 5-5a is the crudest form of numerical integration, with no sub-cell breakdown. This method has no dependence upon n since there are no sub-cell breakdowns involved.

Alone of these equations, 5-2a is the only one which approaches true integration as n approaches infinity. Equation 5-3a will be seen to converge to values very close to those in equation 5-2a; equation 5-4a converges to values smaller than equation 5-2a; equation 5-5a does not converge, but remains constantly lower than equation 5-2a.

Each equation, 5-2b, 5-3b, 5-4b, 5-5b corresponds to the equation above it, but with $S(\psi)$ being interpolated instead of rigorously calculated. As stated in the previous section, the smaller ψ gets, the larger the errors become in the interpolation of $S(\psi)$, so calculation versus interpolation was chosen for the numerical integration. Rapp (1975) suggests using an average $S(\psi)$ value, where $S(\psi)$ is interpolated on a table (equation 5-4b), but, to minimize the errors in the numerical integration computations, equation 5-2a was chosen because of its proximity to true

integration. This unfortunately added time to the computations, and as will be seen later, the trade off of higher accuracy for longer computational time may not be worth the cost.

5.2 Numerical Results

This section will take the information from the previous section and previous chapters and list the actual numerical results of the various computational methods described. The goal of this chapter is to discover two things -- 1) Why was there a 2 meter discrepancy between the given and calculated undulations at 7120 and 7210 in Despotakis (ibid) and 2) What is the best agreement between given and calculated undulations which can be achieved with the numerous variables to be outlined in section 5.2.1.?

5.2.1. Computational Variables

The computation of the Stokes' Integral was used for all cap contributions to the geoid undulation. The corrections to the free-air gravity anomalies have been discussed in chapter 3, and all were applied in the computations.

So far, a number of ways to compute the geoid undulation have been discussed, and some conclusions drawn, but the actual computations will present an idea of how the terrain around Maui and surrounding islands affects the geoid undulation at the laser station, if at all. Certain variables cannot be known with absolute

accuracy, including crustal density, geodetic coordinates, and orthometric heights. For this reason, the following variables were used in the computations:

1) Use two different sets of ellipsoidal coordinates/orthometric heights on two different reference ellipsoids. In the first, the coordinates were given in the SL6 system and converted to the OSU GRS 1987 ellipsoid. This was the method used by Despotakis (ibid), and will hereafter be referred to as the 'old' system. The second set of coordinates are more recent and given in the SL7.1 system and converted to the OSU GRS 1991 ellipsoid, which will be known as the 'new' system.

2) Use two different crustal density assumptions. The first was the mean density for the earth, $2.67 \times 10^3 \text{ kg/m}^3$. The second, a mean density for basalt, based on the volcanic nature of the Hawaiian Islands, $2.9 \times 10^3 \text{ kg/m}^3$. The true mean density may lie between these two values, but as will be shown, this will have only a slight impact (around 1-2 cm) on the final answer.

3) Compute terrain corrections on three different sizes of grids -- $2' \times 2'$, $30'' \times 30''$, and $3'' \times 3''$. These will be used to determine if the data density of $3'' \times 3''$ was necessary to accurately calculate the terrain correction.

4) Use three different spherical harmonic reference fields. The first was OSU86F, used by Despotakis (ibid). The second, OSU89B; and the third, OSU91A. Each field was used to degrees 180 and 360.

5.2.2 Terrain Correction Calculations

The computation of terrain corrections (TC's) was done for three types of elevation data -- 2'x2', 30"x30" and 3"x3" values. All TC's in the 5°x5° area around Hawaii ($18^{\circ} \leq \phi \leq 23^{\circ}$, $201^{\circ} \leq \lambda \leq 206^{\circ}$) were calculated with COGEOIDV, a Fast Fourier Transform (FFT) program, capable of processing 600x600 points, used for TC calculations (Wang, 1991, personal communication). For a complete discussion of the use of FFT's in calculating TC's, see Zhao (1989). The first step in the TC calculations was to develop a 7°x7° elevation file ($17^{\circ} \leq \phi \leq 24^{\circ}$, $200^{\circ} \leq \lambda \leq 207^{\circ}$) with elevations on a 3"x3" grid. Although we only want TC's in the 5°x5° area, we must have extra elevations around the edges for an FFT border. The 3"x3" gridded elevations in the 7°x7° area were derived from the two elevation files, ETOPO5U and DMA DTED (see section 4.4). Because the elevations in ETOPO5U are on a 5'x5' grid, these values were 'spread' onto a 3"x3" grid. By 'spreading' the 5' values, we mean to assume that the given mean elevation in a 5'x5' area is constant over that area, and thus that elevation may be assigned to any point in the 5'x5' area. In areas where 3" elevation data were already available, no changes were made. But in areas without 3" elevation data, each 5'x5' area had its mean elevation (from ETOPO5U) 'spread' onto a 3"x3" grid in that 5'x5' area. Thus in each 5'x5' area, 100x100 elevations ($5'x5'/3"x3"$) of identical value were assigned to every 3"x3" grid point. The 2'x2' and 30"x30" elevations were

these 20'x20' areas, some radically high TC's were occurring (many over 1000 mgals). Because of this, a second method of calculating 3"x3" TC's was used. In this second method, the same 20'x20' area was used, but it was first broken into four 10'x10' areas (200x200 points) with a border of 10' (200 points). It was hoped that this would prevent the 'border error' by buffering the TC's with an FFT border of 200 points. Unfortunately, this was not the case. Even in this second method, the 'border error' occurred, although on a smaller scale (order of 100-200 mgals). Also, in this second method, the edges of the four 10'x10' areas did not always fit neatly to each other. Figure 14 has shown a 20'x20' area whose 3"x3" TC's were processed by method 1. Figure 15 shows the same area, but processed by method 2. Notice the obvious linear offset where the 10'x10' areas meet. This non-matching was not common to all areas. Figure 16 shows an area where 3"x3" TC's were calculated with method 1, and Figure 17 shows the same area with method 2. Notice that in this particular area, in both cases of calculation (3"-1 and 3"-2), that no border problem arises (Figure 16), nor is there any non-matching of edges (Figure 17). This was the case for most areas checked -- that is, border errors in method 1 (3"-1) lead to some non-matching of edges in method 2 (3"-2).

All areas where 3"x3" elevations were originally available (before spreading 5'x5' elevations) had TC's calculated. Also, one 20'x20' area which did not originally contain 3"x3" elevations had 3"x3" TC's calculated in it. This was done specifically because of its closeness (30-70 km) to the laser station. All areas where 3"x3"

derived by averaging the 3"x3" elevation file (covering 7°x7°) into 2' or 30" grid sizes.

In the case of 2'x2' data, The number of TC's calculated was 150 x 150 (5°x5°), with a border of 30 points (1°). This was done with one run of COGEOIDV.

For 30"x30" data, two ways of calculating TC's were used. The first method (30"-1) was to break the 5°x5° area around the station into 4 parts, each containing 300 x 300 points (2.5°x2.5°), with a border of 120 points (1°). This sub-sectioning is shown in Figure 13. Each part was then processed by COGEOIDV, and the 4 parts combined into a 600 x 600 TC file covering the 5°x5° area around the station. This was done because of the limitation of COGEOIDV to processing 600 x 600 points, which includes the border around the points. The second method (30"-2) was to calculate all 600 x 600 TC's (5°x5°) in one run of COGEOIDV. This meant that NO FFT border was put around these points. However, the elevations outside of the 5°x5° area are almost all zero. Therefore, the errors in this method were expected to be minimal. As seen later, there is hardly any difference between these two methods.

Calculating all TC's in the 5°x5° area with one run of COGEOIDV was not possible with the 3"x3" values because it would have had to calculate 6000 x 6000 values. Therefore, for 3"x3" TC's, 2 methods were used. For the first method, areas of 400 x 400 points (20' x 20') with a border of 100 points (5') were processed with each run of COGEOIDV. Initial plots of these terrain corrections revealed a 'border error' in some areas (see Figure 14). Along the edges of

TC's were calculated are shown on Figure 18, with corresponding code numbers for each area. The justification for calculating 3"x3" TC's in an area where only 5'x5' elevations were available can be made because this area contains no crustal masses above sea level (i.e. it is completely water covered), thus all elevations above sea level in this 20'x20' area are zero. The only areas which surround this area and which have crustal masses above sea level, are those areas which originally had 3"x3" elevations available. Thus, no error should be introduced in the calculation of 3"x3" TC's in this area, because all elevations (whether on 3" or 5' grid) in this area are zero. Finally, in those areas where 3" TC's were not calculated, 2' TC's were used.

Thus, in the program to calculate the cap contribution, the sub-cell breakdown was 1600 sub-cells in those areas outlined with heavy dark lines in Figure 18, and 1 sub-cell in all other areas.

Although the use of 30" or 2' elevation data does not require the 1600 sub-cell breakdown which is used with the 3" data, this sub-cell breakdown was maintained for 2', 30" and 3" TC's so that no effects of different computational schemes would enter the undulation computations.

To alleviate the problem of the border error, a 'filter' was applied to the 20'x20' areas containing 3"x3" TC's. This filter would examine the TC's along the edge of the 20'x20' area for values of TC larger than 100 mgals. If TC's above 100 mgal were found, they were set to zero. Admittedly, this is not a very accurate way to alleviate the problem, and in the future, it may be useful to

examine ways to properly remove the border problem. It will first become necessary to fully understand the cause of the problem. It may be that the border error is not caused only by using too small of an FFT border for the computations.

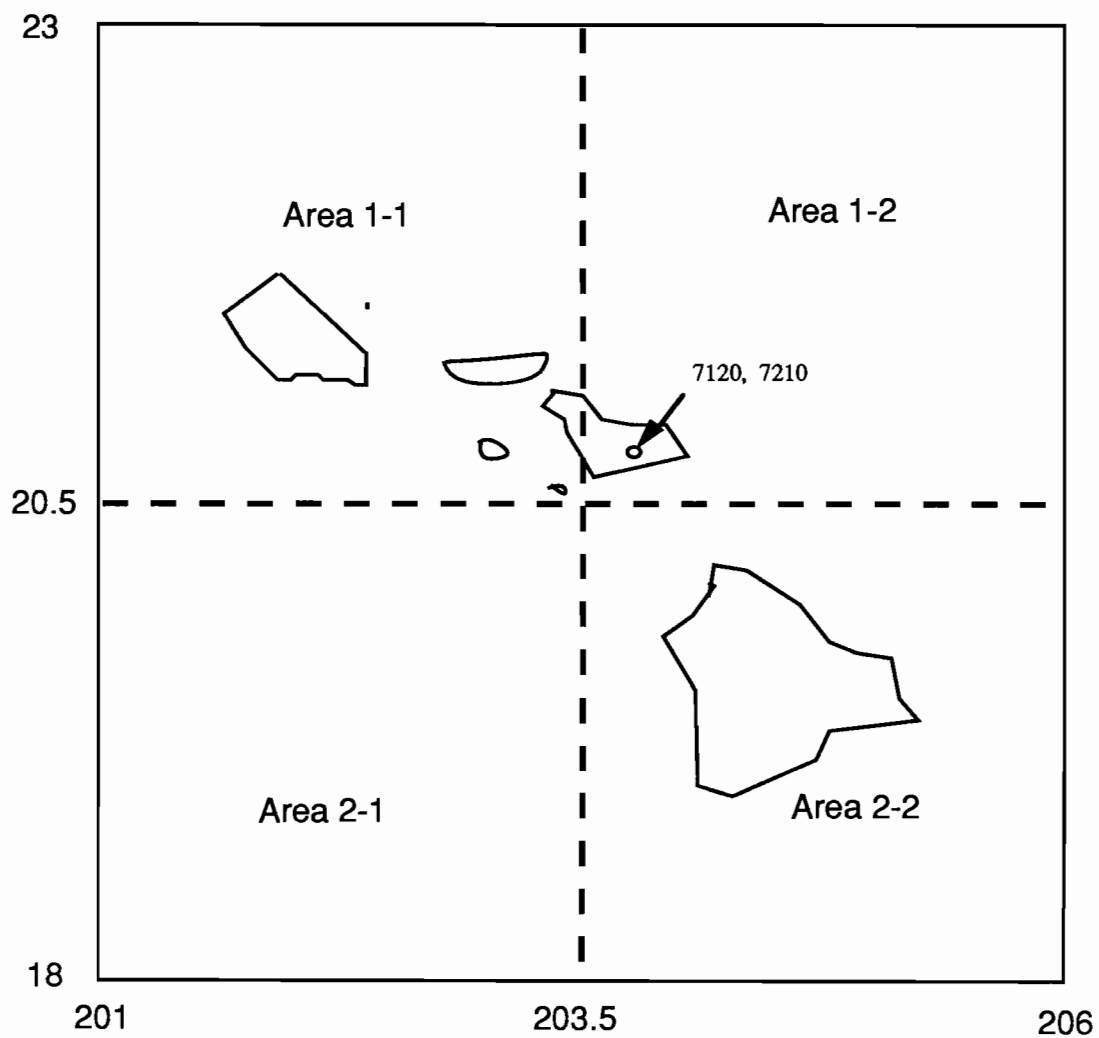


FIGURE 13

Division of 5°x5° area into 4 parts for 30"x30" TC calculation,
(method #1)

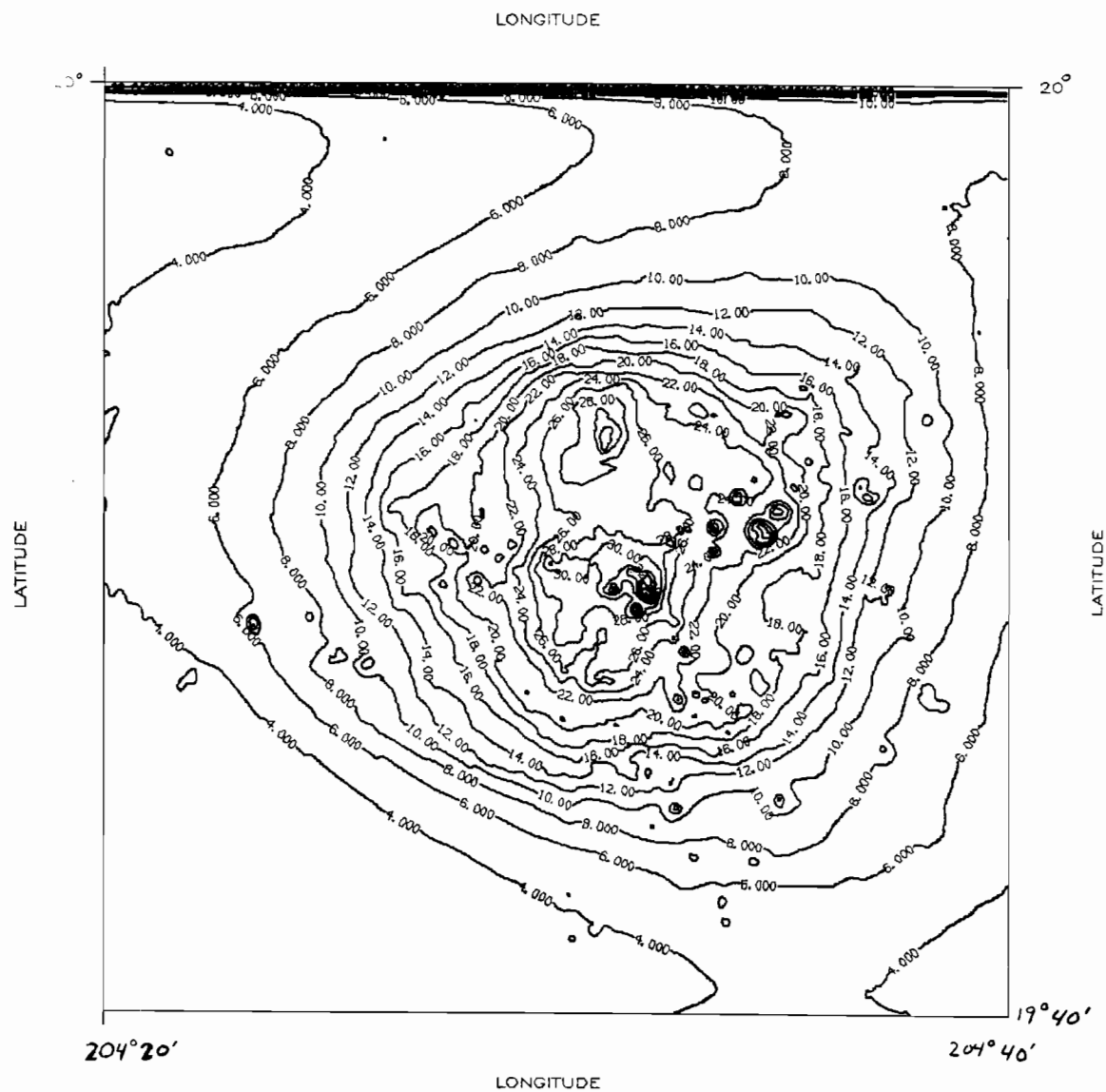


FIGURE 14

3'' Terrain corrections, using 20'x20' FFT with 5' border, $CI=2\text{mgal}$,
 Area surrounding Mt. Mauna Kea (Code number 2.12)

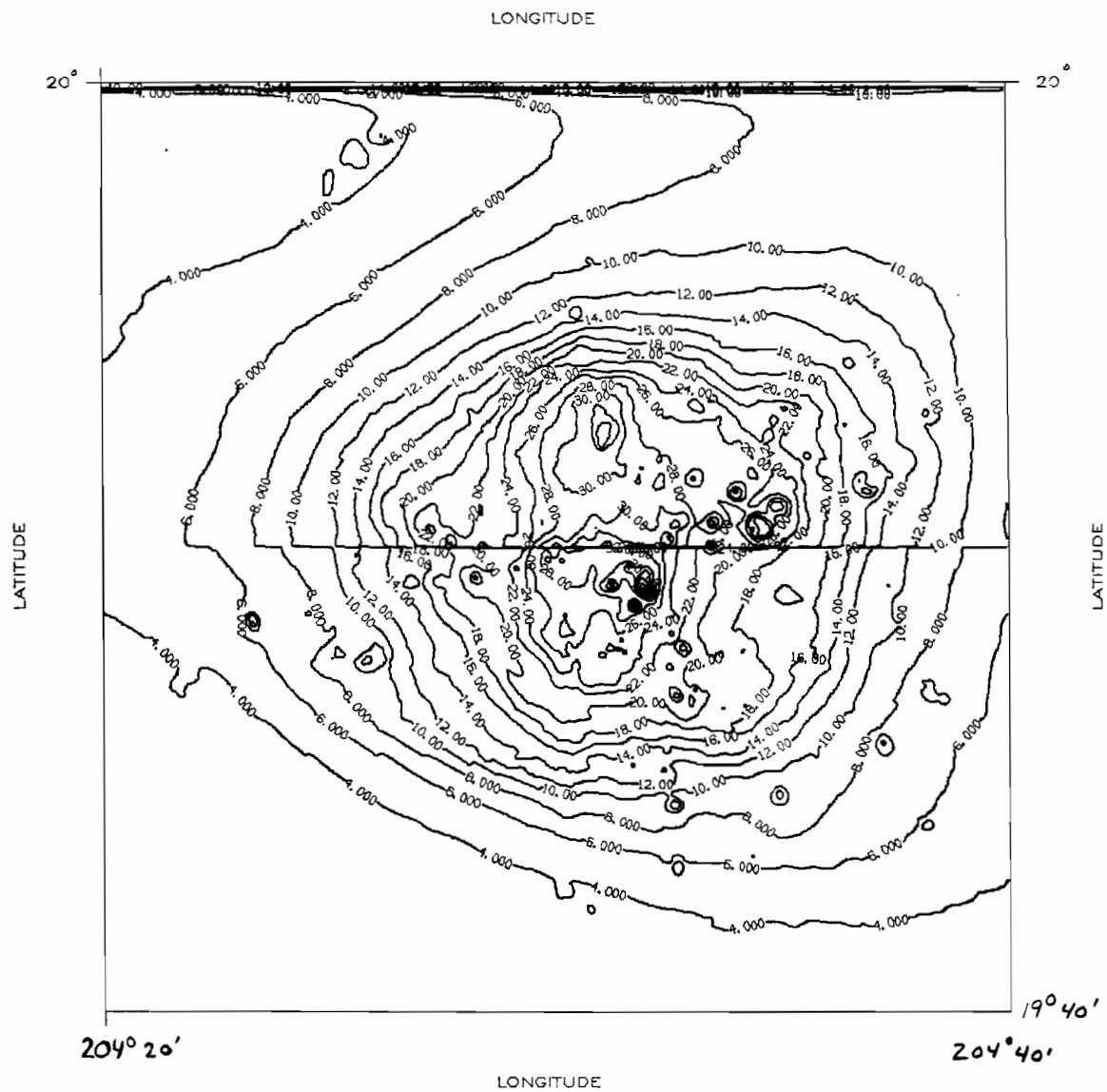


FIGURE 15

3" Terrain corrections, using 10'x10' FFT with 10' border, CI=2mgal
 Area surrounding Mt. Mauna Kea (Code number 2.12)

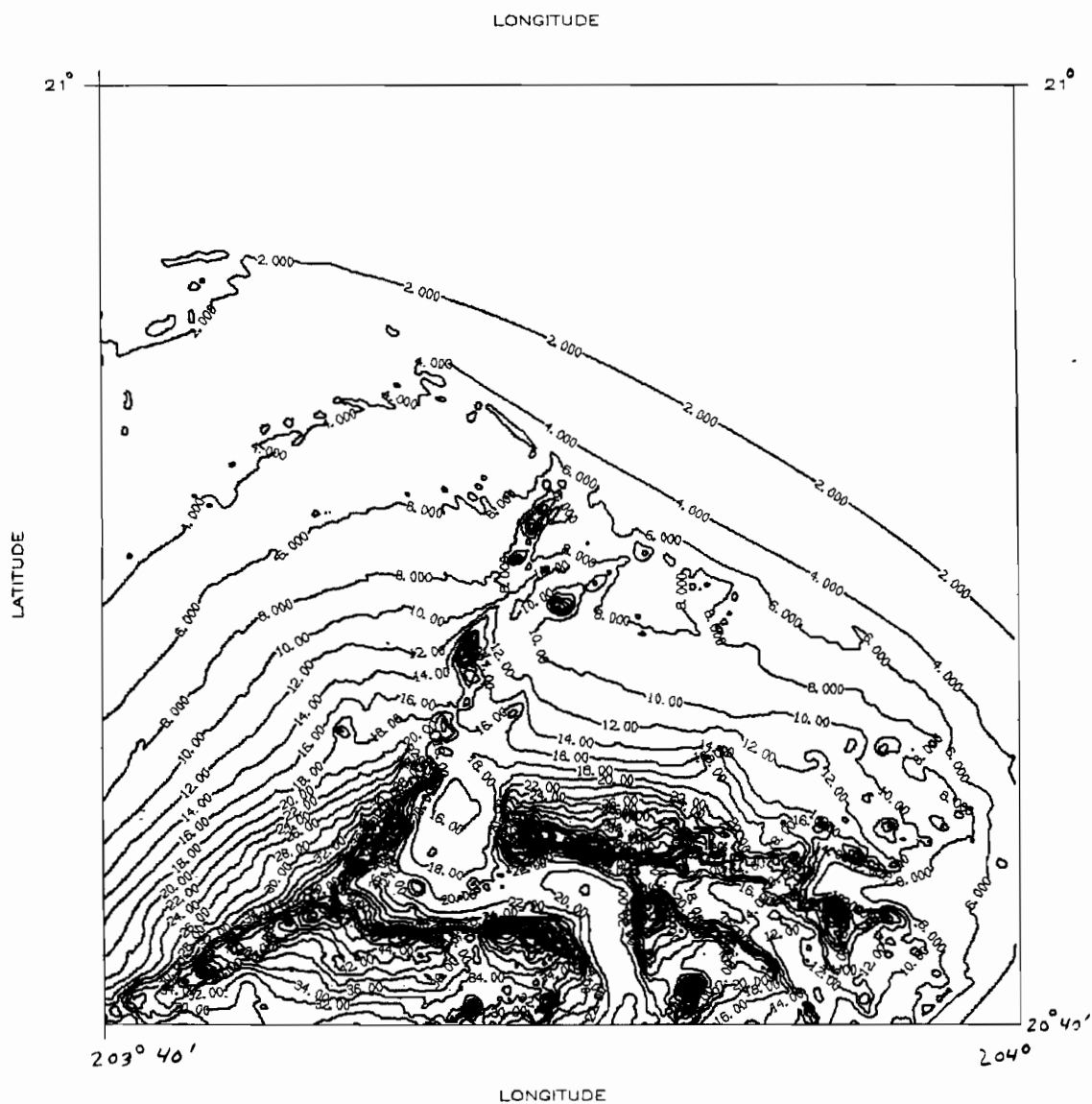


FIGURE 16

3'' Terrain corrections, using 20'x20' FFT with 5' border, $CI=2\text{mgal}$
 Area surrounding Mt. Haleakala (Code number 5.13)

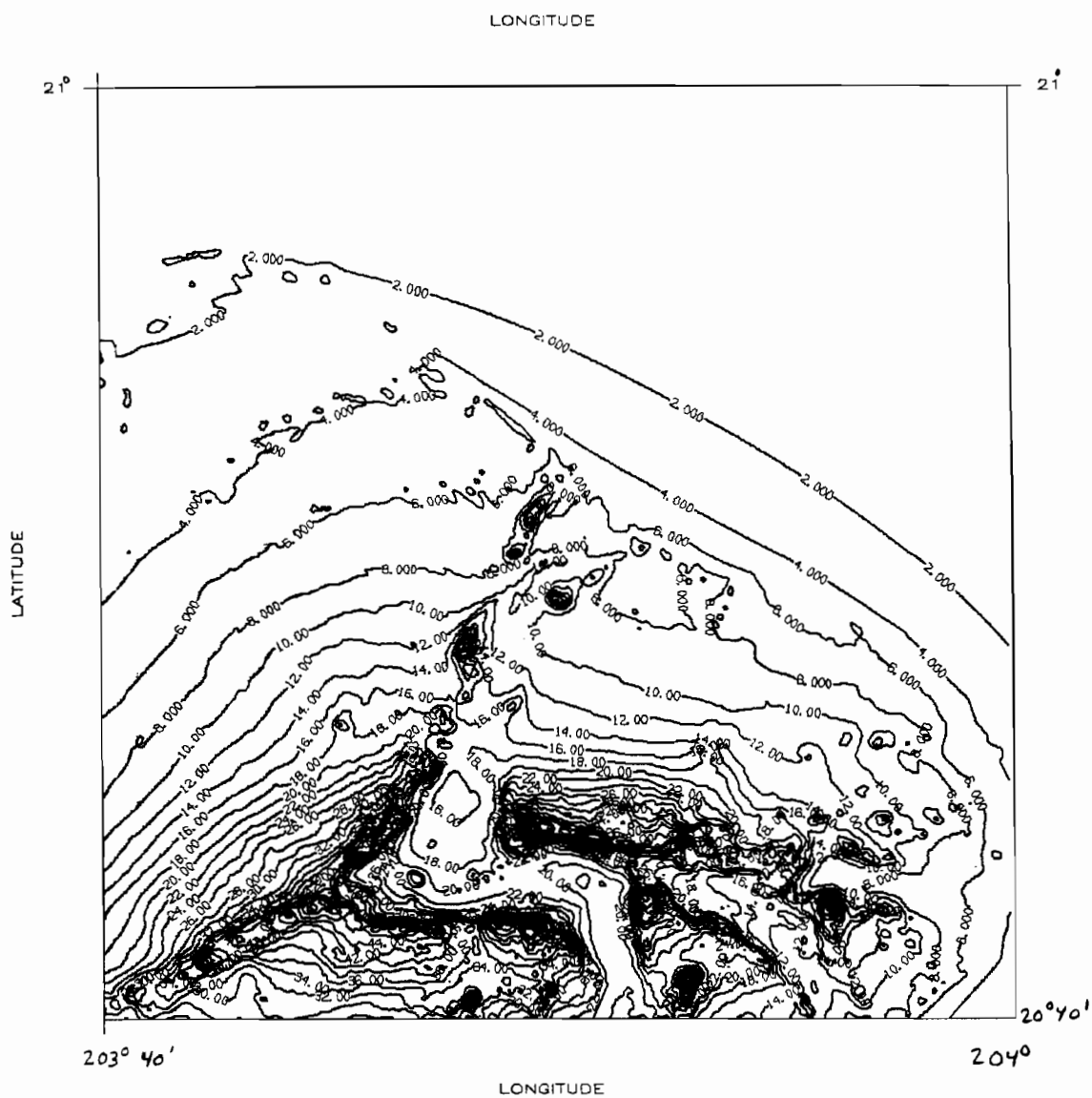


FIGURE 17

3" Terrain corrections, using 10'x10' FFT with 10' border, CI=2mgal
Area surrounding Mt. Haleakala (Code number 5.13)

Tables 6 and 7 show the average, standard deviation, RMS, maximum and minimum values for the TC's over land and over seas which are associated with each grid size used in the computation of the TC's. In those cases where the TC's were calculated in areas smaller than $5^{\circ} \times 5^{\circ}$ ($30''-1$ and $3''-1$ and $3''-2$), the statistical values for each individual file are not shown, only the overall values.

It will be important in the rest of this report to know which terrain corrections are most accurate. As a method of comparison, two references were used. Mt. Mauna Kea, on the island of Hawaii, has a rigorously calculated (using rings) terrain correction of 36 mgals (Heiskanen and Vening Meinesz, 1958). This value was also rigorously calculated by a program known as TC (Forsberg, 1984) which calculates terrain corrections by prism formulas. The value computed by TC was 43.6 mgals. The data used in this calculation were $3''$ elevations inside a radius of 30 km, and $2'$ elevations from 30 km out to 200 km. Since no detailed information concerning the exact source of the data used by Heiskanen and Vening Meinesz was available, we assume the more accurate value comes from the TC program, 43.6 mgals. Therefore, we will look for the terrain correction calculation which best fits this particular value. Figure 19 is an elevation plot of $3''$ elevations in the $20' \times 20'$ area around Mt. Mauna Kea. The corresponding TC plot was previously shown as Figure 14 (and Figure 15). Figure 20 shows elevations in the same area, but on a $30'' \times 30''$ mean grid. Lastly, Figure 21 shows the $30'' \times 30''$ TC's in this area. Notice, first, that the TC plot is

smoother for the 30" elevations than it is for the 3" elevations. This is as expected, since the 30" elevations are mean values of the 3" elevations. However, notice that in Figure 14 (3" TC's), the TC associated with Mt. Mauna Kea is only 42.2 mgals, but in Figure 21 (30" TC's) the TC is 55.9 mgals. Thus, when using FFT for the calculation of terrain corrections, the 3" elevations yield better accuracy, even though they disregard data outside of their small (20'x20' or 10'x10') computational areas.

TABLE 6

Statistical values of terrain corrections over land areas (mgal),
 $\rho=2.67 \times 10^3 \text{ kg/m}^3$

TC's	Average	Std. Dev.	RMS	Min	Max
2'x2'	6.88	7.02	9.83	0.05	50.10
30"-1	7.93	7.62	11.00	0.09	59.90
30"-2	7.94	7.63	11.01	0.09	59.75
3"-1	6.61	7.08	8.82	0.03	79.00
3"-2	6.15	6.97	8.49	0.06	79.15

TABLE 7

Statistical values of terrain corrections over sea areas (mgal),
 $\rho=2.67 \times 10^3 \text{ kg/m}^3$

TC's	Average	Std. Dev.	RMS	Min	Max
2'x2'	0.11	0.32	0.34	0.00	6.10
30"-1	0.12	0.38	0.40	0.00	10.65
30"-2	0.13	0.38	0.40	0.01	10.60
3"-1	0.32	1.09	1.03	0.00	42.14
3"-2	0.21	0.71	0.71	0.00	45.37

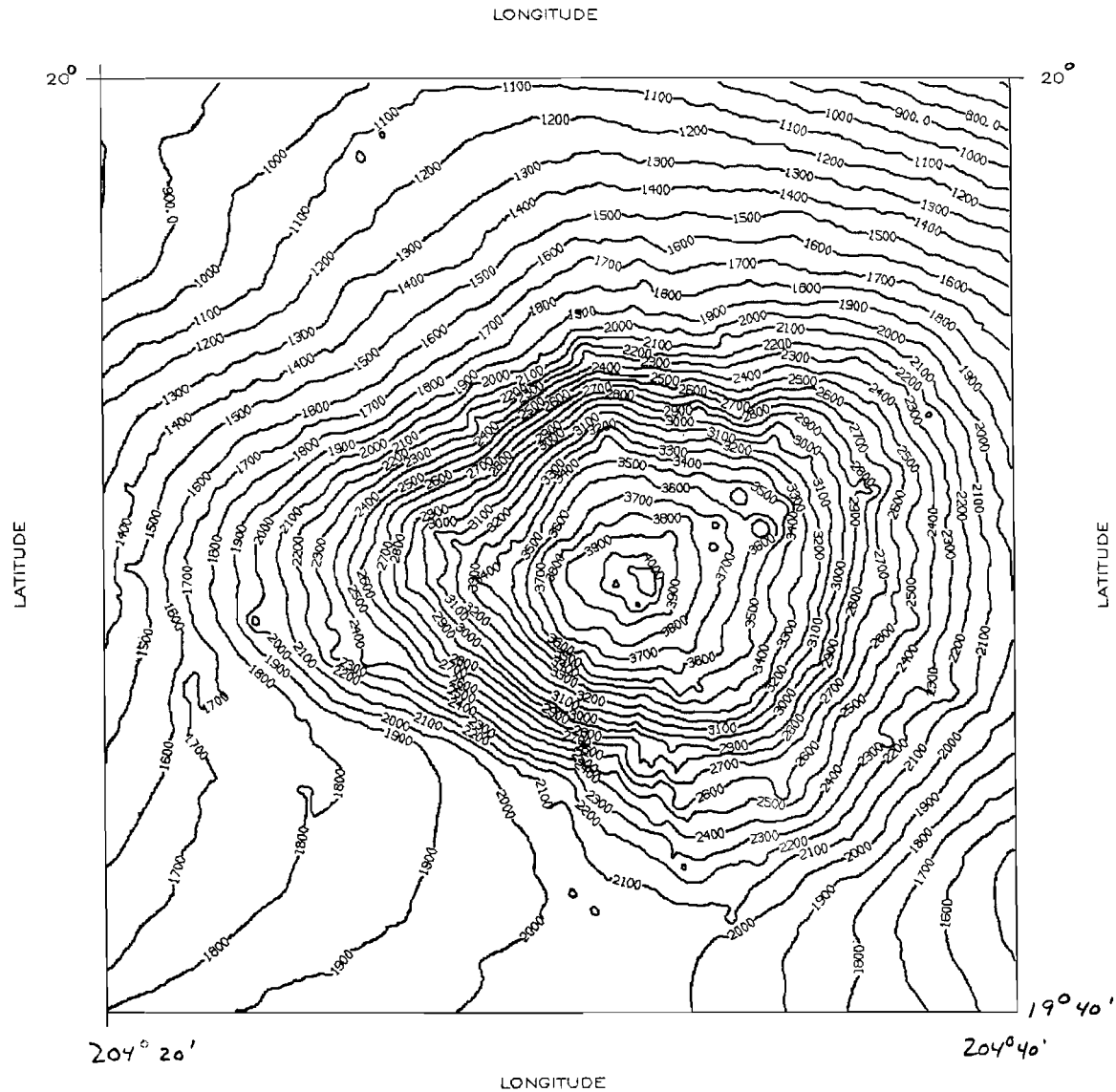


FIGURE 19

Elevation plot around Mauna Kea using 3" elevations, CI=100 m
(Code number 2.12)

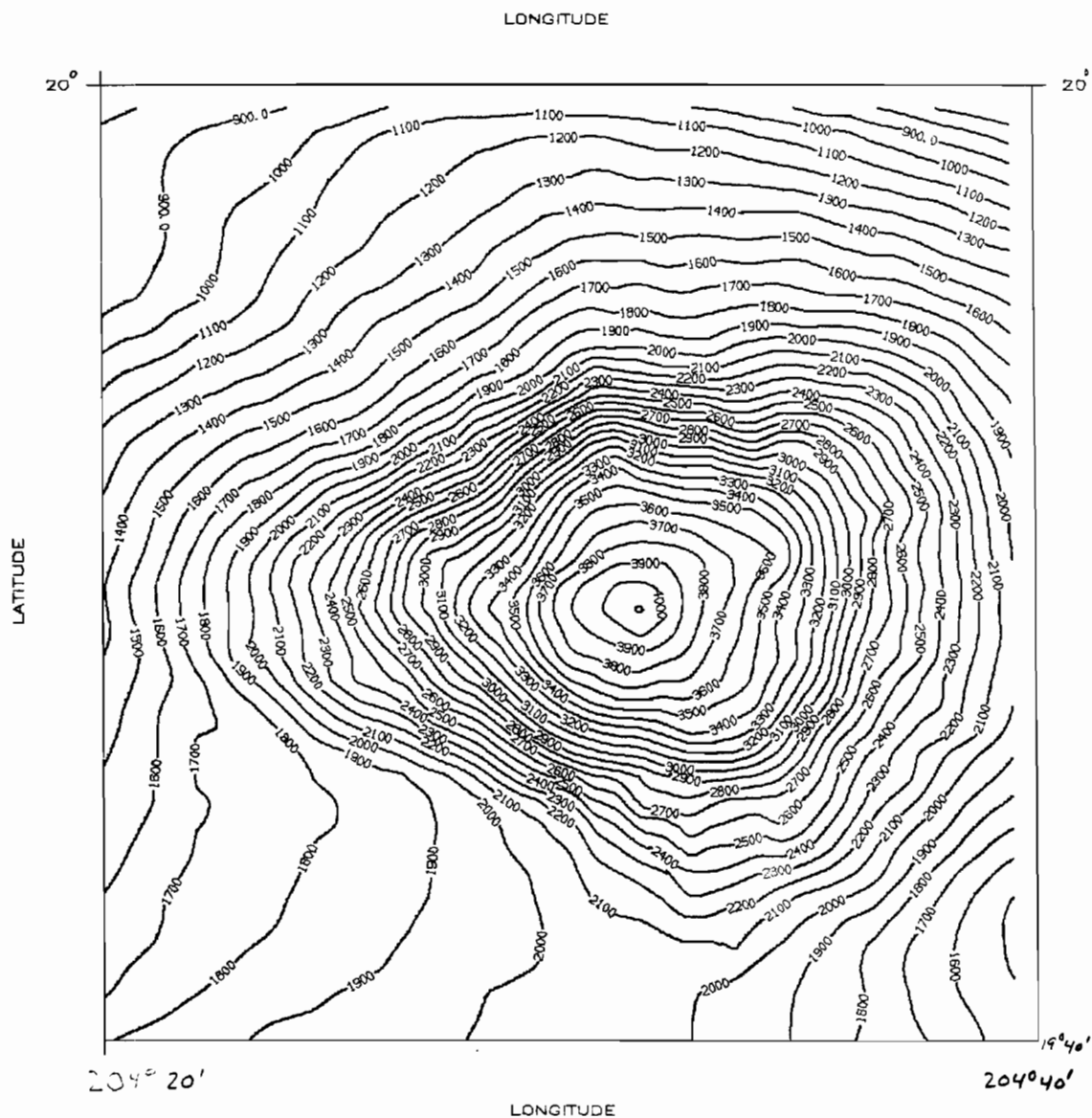


FIGURE 20

Elevation plot around Mauna Kea using 30" elevations, CI=100 m
(Code number 2.12)

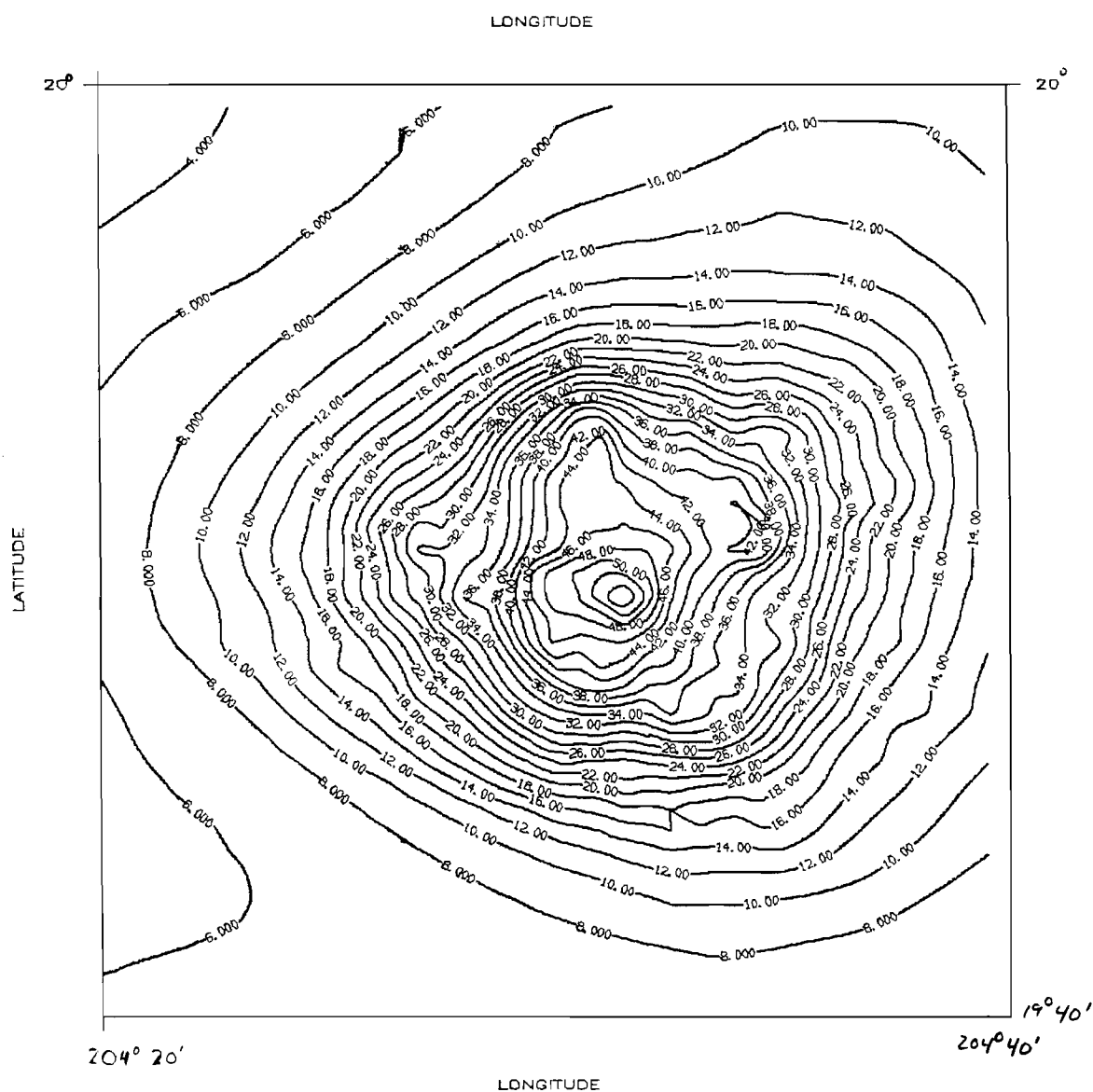


FIGURE 21

Terrain correction plot around Mauna Kea using 30" TC's, $Cl=2$ mgal
(Code number 2.12)

5.2.2.1 The Crustal Density

As the time approaches when the precision of geoid calculations approaches the centimeter level, certain fundamentally accepted assumptions will need to be re-examined for their applicability. One of those assumptions is the density of the crust of the earth. The commonly accepted value of $2.67 \times 10^3 \text{ kg/m}^3$ is not acceptable for use in the area of the Hawaiian islands¹. Although no true mean value is known for the area, due to the volcanic nature of the islands, it is reasonable to assume that the density of basalt ($2.9 \times 10^3 \text{ kg/m}^3$) is near the mean value of all crustal masses above the geoid in the integration cap.

The most accurate way to treat the crustal density in geoid calculations would be to have a density model relative to geodetic coordinates which would yield higher accuracy in terrain corrections by leaving density inside the integration instead of assuming a mean value and moving density outside of the integration. However, no such crustal density model was available, and thus the possible mean values of 2.67×10^3 and $2.9 \times 10^3 \text{ kg/m}^3$ were both used for comparison.

Unquestionably, the most time consuming calculations done in this report were the terrain corrections. Fast Fourier Transform methods were used to calculate terrain corrections, yet dozens of computer hours still went into these calculations due to the dense

¹ Professor Ralph Von Frees, Department of Geological Sciences, The Ohio State University, Personal Communication

nature of the elevations. Because terrain correction calculations require a crustal density assumption, it became important to develop a simple way to calculate TC's with a new density assumption, without needing to run another FFT program. Equation 5-6 shows the dependence upon density assumptions made in the cap integration of the Stokes' integral:

$$N_{\text{cap}}(\rho_1) = \frac{R}{4\pi\gamma} \iint_{\sigma_c} (\Delta g + \text{TC}(\rho_1) + \delta g_{\text{sl}}(\rho_1) + \delta g_A) S(\psi) d\sigma + \delta N_I(\rho_1) \quad (5-6)$$

where:

Δg Free-air gravity anomalies

which may be written in the following notation:

$$N_{\text{cap}_2} = N_{\Delta g} + \delta N_{\text{TC}_2} + \delta N_{\delta g_{\text{sl}_1}} + \delta N_A + \delta N_{I_z} \quad (5-7)$$

where:

$$N_{\Delta g} = \frac{R}{4\pi\gamma} \iint_{\sigma_c} \Delta g S(\psi) d\sigma \quad (5-8)$$

$$\delta N_{\text{TC}_1} = \frac{R}{4\pi\gamma} \iint_{\sigma_c} \text{TC}(\rho_1) S(\psi) d\sigma \quad (5-9)$$

$$\delta N_{\delta g_{sl_1}} = \frac{R}{4\pi\gamma} \iint_{\sigma_c} \delta g_{sl}(\rho_1) S(\psi) d\sigma \quad (5-10)$$

$$\delta N_A = \frac{R}{4\pi\gamma} \iint_{\sigma_c} \delta g_A S(\psi) d\sigma \quad (5-11)$$

$$\delta N_{I_1} = \frac{-\pi G \rho_1 H^2}{g} \quad (5-12)$$

Equations 5-9, 5-10 and 5-12 are all dependent upon the crustal density assumption made. It is unreasonable to recreate the entire calculations of these quantities if a simple transformation is available. Looking at the equations for terrain correction, secondary indirect effect and indirect effect, we see:

$$TC_1 = \frac{1}{2} G \rho_1 \int_{-\infty}^{+\infty} \int_{-\infty}^{+\infty} \frac{(h-h_p)^2}{d^3} dx dy \quad (5-13)$$

$$\delta g_{sl_1} = .3086 \delta N_{I_1} = .3086 \left[\frac{-\pi G \rho_1 H^2}{\gamma} \right] \quad (5-14)$$

$$\delta N_{I_1} = \frac{-\pi G \rho_1 H^2}{\gamma} \quad (5-15)$$

Notice that each of these is linearly dependent upon the density assumption made. Thus, to calculate quickly the new values of

terrain correction, secondary indirect effect and indirect effect with a new mean crustal density assumption, one can use the following equations:

$$TC_2 = \frac{\rho_2}{\rho_1} TC_1 \quad (5-16)$$

$$\delta g_{SI_2} = \frac{\rho_2}{\rho_1} \delta g_{SI_1} \quad (5-17)$$

$$\delta N_{I_2} = \frac{\rho_2}{\rho_1} \delta N_{I_1} \quad (5-18)$$

Thus, if the cap contribution to the geoid undulation is calculated once for a known density, and each component part (equations 5-8 through 5-12) is known, then it is a simple matter to re-calculate quickly the cap contribution using any other density. Equation 5-19 shows the basic formula for cap contribution with density ρ_2 :

$$N_{cap_2} = N_{\Delta g} + \delta N_{TC_2} + \delta N_{\delta g_{SI_2}} + \delta N_A + \delta N_{I_2} \quad (5-19)$$

but this may be written in terms of precalculated values using density ρ_1 :

$$N_{\text{cap}_2} = N_{\Delta g} + \frac{\rho_2}{\rho_1} \delta N_{\text{TC}_1} + \frac{\rho_2}{\rho_1} \delta N_{\delta g_1} + \delta N_A + \frac{\rho_2}{\rho_1} \delta N_{I_1} \quad (5-20)$$

Equation (5-20) will be very useful in determining the effect on geoid undulations assuming a crustal density other than $2.67 \times 10^3 \text{ kg/m}^3$.

5.2.3 Local Average Correction

The terrestrial mean anomalies used in the calculation of the cap contribution to the geoid undulation may differ from the mean anomalies implied by the potential coefficient model used in the outer zone calculation through the following equation (Despotakis, *ibid*, p. 81):

$$\widehat{\Delta g}^T = \widehat{\Delta g}^S + \delta(\Delta g^S) \quad (5-21)$$

where:

$\widehat{\Delta g}^T$ Terrestrial mean anomaly (or terrain corrected terrestrial mean anomaly, if TC's are used)

$\widehat{\Delta g}^S$ Mean anomaly implied by a potential coefficient model

For a complete derivation of the equations used, see Despotakis (ibid, p. 81-86).

For now, we will present the numerical results of the local average correction without the use of terrain corrections. We will see that the calculations show that without terrain corrections the local average correction is inapplicable in this area, and if terrain corrections are applied, the results become even worse.

The formula for the local average correction (using the original Stokes' integral) is:

$$\delta N^0 = -\frac{R}{2\gamma} \left(\Delta g_0^P - \Delta g_0^T \right) Q_0 \quad (5-22)$$

where:

Δg_0^T Average of terrestrial mean anomalies inside integration cap

Δg_0^P Average of potential coefficient model (PCM) mean anomalies inside integration cap

The value of Q_0 ($\psi_c = 2^\circ$) is:

$$Q_0 (\psi_c = 2^\circ) = -0.075620$$

So that the corresponding local average correction, a , in m/mgal of the correction δN^0 is

$$a=0.0245854 \text{ m/mgal}$$

Thus, the computation of δN^0 is done by:

$$\delta N^0 = a \left(\Delta g_0^P - \Delta g_0^T \right) \quad (5-23)$$

Before listing the numerical values, it is necessary to mention that the values listed for the average anomalies in the Hawaiian area in Despotakis (ibid, p. 61) are incorrect. Those averages were taken over a $5^\circ \times 5^\circ$ area surrounding the laser stations, not over the integration cap itself. The difference, as will be seen, is significant.

The numerical values of the average anomalies are shown in Table 8 below. For simplicity, not all reference fields, maximum degrees of expansion, nor ellipsoids are used. Conclusions can be drawn from just the information listed below:

TABLE 8
Terrestrial and PCM mean anomalies and their respective local
average corrections

Old System		
Δg_0^T	OSU86F (to 180)	OSU86F (to 360)
46.68 mgal	$\Delta g_0^P = 39.33 \text{ mgal}$ $\Delta g_0^P - \Delta g_0^T = -7.35$ mgal $\delta N^0 = -1.807 \text{ m}$	$\Delta g_0^P = 41.29 \text{ mgal}$ $\Delta g_0^P - \Delta g_0^T = -5.39$ mgal $\delta N^0 = -1.325 \text{ m}$
New System		
Δg_0^T	OSU91A (to 180)	OSU91A (to 360)
46.78 mgal	$\Delta g_0^P = 37.23 \text{ mgal}$ $\Delta g_0^P - \Delta g_0^T = -9.55$ mgal $\delta N^0 = -2.348 \text{ m}$	$\Delta g_0^P = 39.42 \text{ mgal}$ $\Delta g_0^P - \Delta g_0^T = -7.36$ mgal $\delta N^0 = -1.809 \text{ m}$

In Despotakis, the values of Δg_0^T , Δg_0^P and δN^0 were:

$$\Delta g_0^T = 25.30 \text{ mgal}$$

$$\Delta g_0^P = 23.21 \text{ mgal}$$

$$\delta N^0 = -0.513 \text{ m}$$

which are obviously quite different from the values above for OSU86F (to 180) in the old system. This difference is strictly from averaging over a $5^\circ \times 5^\circ$ area, instead of restricting the averaging over the cap only.

Note that the anomalies used above do not include the mean terrain corrections. If these values were added to the terrestrial mean anomalies, the difference $\Delta g_0^P - \Delta g_0^T$ would approach 15 mgal, which would subsequently lead to local average corrections of magnitude 3-4 meters.

Despotakis assumed that the terrestrial mean anomalies were in error from those anomalies implied by the reference field. However, as seen above, this assumption yields 'corrections' which severely alter the calculated undulation, and therefore are considered inapplicable for this area, and will be ignored. Additional study is warranted on the validity of the local average correction.

5.2.4 The Cap Calculations

Table 9 shows the cap contribution to the geoid undulation (hereafter just called the cap contribution) by using free-air gravity anomalies alone. All 8 possible numerical integration equations were used (see section 5.1.1.4), using the original sub-cell breakdown (section 5.1.1.2). The outlined values correspond to the method reported by Despotakis (ibid), before applying local average corrections. However, as mentioned earlier, Despotakis' cap contributions were too low by around 20 cm due to an error in his computer program (see section 5.1.1.1), and therefore his reported values do not agree with the values on Table 9. Table 10 contains the same information as Table 9, but using the 1600 sub-cell breakdown of Figure 18. The outlined values are those used in this study. Both the old and new reference systems are shown in these tables.

Looking at Tables 9 and 10, some things became obvious immediately :

First, the difference between interpolating and calculating the Stokes' function is minimal. Even though the errors in $S(\psi)$ are very large near the station, they are not large enough to affect significantly the calculated undulation. The largest difference seen is 4 mm. Also, the difference between equations 5-2a, 5-2b, 5-3a and 5-3b is very small. Thus, for the calculation of the cap contribution, equation 5-3b (used by Despotakis, ibid) would be nearly as accurate as 5-2a (used in this study). Equation 5-2a was

chosen in this study as the best possible estimate to true integration - the very smallest errors possible due to computational methods were wanted, so that the emphasis of this study could be on the effects of terrain, not the effects of computational methods. But for calculations where errors due to computational methods can be less than 1cm, equation 5-3b would be the best choice, as it takes much less computer time, and yields results extremely close to 5-2a.

Equations 5-4a and 5-4b were investigated as a possible way to avoid lengthy computations, in the same way as equations 5-3a and 5-3b. However, the results of 5-4a and 5-4b yield poorer results than a crude integration using no sub-cells (equations 5-5a, 5-5b). Obviously they are insufficient for use in geoid computations.

When calculating the contribution of the terrain corrections to the cap calculation (N_{TC} , Equation 5-9), for 3" (both methods), 30" (both methods) and 2' elevation files, one expects the denser 3" data to contain more information about the irregularities in the terrain, and thus to have the most accurate values of N_{TC} .

TABLE 9

Cap contribution from free-air gravity anomalies using $\Delta\sigma$
breakdown of Despotakis (64-16-4-1 sub-cells)

	Old Reference Ellipsoid		New Reference Ellipsoid	
	7120	7210	7120	7210
Eqn. 5-2a	20.967 m	20.995 m	20.990 m	21.018 m
5-2b	20.968	20.998	20.990	21.020
5-3a	20.967	20.995	20.990	21.017
5-3b	20.968	20.998	20.990	21.020
5-4a	20.540	20.535	20.563	20.558
5-4b	20.540	20.535	20.563	20.558
5-5a	20.898	20.882	20.931	20.914
5-5b	20.898	20.882	20.931	20.914

TABLE 10

Cap contribution from free-air gravity anomalies using new $\Delta\sigma$
breakdown (1600 sub-cells)

	Old Reference Ellipsoid		New Reference Ellipsoid	
	7120	7210	7120	7210
Eqn. 5-2a	20.986 m	20.985 m	21.008 m	21.007m
5-2b	20.989	20.988	21.011	21.011
5-3a	20.986	20.985	21.008	21.007
5-3b	20.989	20.988	21.011	21.011
5-4a	20.532	20.527	20.555	20.550
5-4b	20.532	20.527	20.555	20.550
5-5a	20.898	20.882	20.931	20.914
5-5b	20.898	20.882	20.931	20.914

Table 11 contains the values of N_{TC} for 3" (both methods), 30" (both methods) and 2' elevation files in both the old and new system, assuming possible crustal densities of $2.67 \times 10^3 \text{ kg/m}^3$ and $2.9 \times 10^3 \text{ kg/m}^3$. Remember that the 3" TC's were not calculated over the whole cap, and that 2' TC's were used in those areas where 3" TC's weren't calculated. The values of N_{TC} were identical (to the mm) for both the old and new reference systems, and so no distinction is made on Table 11 between them.

Tables 12 and 13 show all elements of the cap contribution, and their sum for the values of $\rho = 2.67 \times 10^3 \text{ kg/m}^3$ and $\rho = 2.9 \times 10^3 \text{ kg/m}^3$.

TABLE 11

Terrain correction contributions to the geoid undulation cap
calculation (N_{TC})

<u>TC procedure</u> Grid interval (-method)	<u>Density</u> ρ (kg/m ³)	<u>Station</u> (in either old or new system)	
		7120	7210
3"/2'-1	2.67×10^3	0.547 m	0.548 m
3"/2'-2	"	0.532	0.532
30" - 1	"	0.653	0.653
30" - 2	"	0.653	0.654
2'	"	0.572	0.572
3"/2'-1	2.9×10^3	0.594 m	0.594 m
3"/2'-2	"	0.578	0.578
30" - 1	"	0.709	0.709
30" - 2	"	0.709	0.710
2'	"	0.621	0.621

TABLE 12

Cap contribution to the geoid undulation, in meters, $\rho=2.67 \times 10^3$
 kg/m^3

Ellip.	Sta.	Elev's	$N_{\Delta g}$	N_{TC}	$N_{\delta g_A}$	$N_{\delta g_{SI}}$	δN_I	N_{CAP}
OSU87	7120	3" - 1	20.986	0.547	0.206	-0.001	-0.531	21.207
"	"	3" - 2	20.986	0.532	0.206	-0.001	-0.531	21.192
"	"	30" - 1	20.986	0.653	0.209	-0.001	-0.531	21.316
"	"	30" - 2	20.986	0.653	0.209	-0.001	-0.531	21.316
"	"	2'	20.986	0.572	0.209	-0.001	-0.531	21.235
"	7210	3" - 1	20.985	0.548	0.206	-0.001	-0.531	21.207
"	"	3" - 2	20.985	0.532	0.206	-0.001	-0.531	21.191
"	"	30" - 1	20.985	0.653	0.209	-0.001	-0.531	21.315
"	"	30" - 2	20.985	0.654	0.209	-0.001	-0.531	21.316
"	"	2'	20.985	0.572	0.209	-0.001	-0.531	21.234
OSU91	7120	3" - 1	21.008	0.547	0.206	-0.001	-0.531	21.229
"	"	3" - 2	21.008	0.532	0.206	-0.001	-0.531	21.214
"	"	30" - 1	21.008	0.653	0.209	-0.001	-0.531	21.338
"	"	30" - 2	21.008	0.653	0.209	-0.001	-0.531	21.338
"	"	2'	21.008	0.572	0.209	-0.001	-0.531	21.257
"	7210	3" - 1	21.007	0.548	0.206	-0.001	-0.531	21.229
"	"	3" - 2	21.007	0.532	0.206	-0.001	-0.531	21.213
"	"	30" - 1	21.007	0.653	0.209	-0.001	-0.531	21.336
"	"	30" - 2	21.007	0.654	0.209	-0.001	-0.531	21.337
"	"	2'	21.007	0.572	0.209	-0.001	-0.531	21.256

TABLE 13

Cap contribution to the geoid undulation, in meters, $\rho=2.9 \times 10^3$
 kg/m^3

Ellip.	Sta.	Elev's	$N_{\Delta g}$	N_{TC}	$N_{\delta g_A}$	$N_{\delta g_{SI}}$	δN_I	N_{CAP}
OSU87	7120	3" - 1	20.986	0.594	0.206	-0.002	-0.577	21.207
"	"	3" - 2	20.986	0.578	0.206	-0.002	-0.577	21.191
"	"	30" - 1	20.986	0.709	0.209	-0.002	-0.577	21.325
"	"	30" - 2	20.986	0.709	0.209	-0.002	-0.577	21.325
"	"	2'	20.986	0.621	0.209	-0.002	-0.577	21.237
"	7210	3" - 1	20.985	0.595	0.206	-0.002	-0.577	21.207
"	"	3" - 2	20.985	0.578	0.206	-0.002	-0.577	21.190
"	"	30" - 1	20.985	0.709	0.209	-0.002	-0.577	21.324
"	"	30" - 2	20.985	0.710	0.209	-0.002	-0.577	21.325
"	"	2'	20.985	0.621	0.209	-0.002	-0.577	21.236
OSU91	7120	3" - 1	21.008	0.594	0.206	-0.002	-0.577	21.229
"	"	3" - 2	21.008	0.578	0.206	-0.002	-0.577	21.213
"	"	30" - 1	21.008	0.709	0.209	-0.002	-0.577	21.347
"	"	30" - 2	21.008	0.709	0.209	-0.002	-0.577	21.347
"	"	2'	21.008	0.621	0.209	-0.002	-0.577	21.259
"	7210	3" - 1	21.007	0.595	0.206	-0.002	-0.577	21.229
"	"	3" - 2	21.007	0.578	0.206	-0.002	-0.577	21.212
"	"	30" - 1	21.007	0.709	0.209	-0.002	-0.577	21.346
"	"	30" - 1	21.007	0.710	0.209	-0.002	-0.577	21.347
"	"	2'	21.007	0.621	0.209	-0.002	-0.577	21.258

5.2.5 The Outer Zone Calculations

As outlined in Chapter 2, the calculation of the outer zone effect is done using spherical harmonic reference fields.

Table 14 shows the results of the outer zone calculations (equation 2-7) when using the three different reference fields to degrees 180 and 360 in both the old and new system.

TABLE 14
Outer zone contribution (meters) to the geoid undulation

		Model					
		OSU 86 F		OSU 89 B		OSU 91 A	
Ellip.	Sta.	180	360	180	360	180	360
OSU87	7120	-1.830	-2.023	-1.035	-1.244	-0.929	-1.139
"	7210	-1.831	-2.023	-1.035	-1.244	-0.929	-1.139
OSU91	7120	-1.830	-2.023	-1.034	-1.244	-0.929	-1.139
"	7210	-1.831	-2.023	-1.035	-1.244	-0.929	-1.139

5.2.5.1 Ellipsoidal Corrections

The calculation of the geoid undulation through Stokes' integral is in error because it is in spherical approximation, instead of ellipsoidal. Therefore, ellipsoidal corrections need to be calculated to correct for this spherical approximation. The exact equations and software used in Despotakis (ibid, p 73-80) were used in this calculation, and ellipsoidal corrections were calculated using all three potential coefficient models used in this study.

Despotakis (ibid) calculated the ellipsoidal corrections to the Stokes' integral using OSU86F up to degree 36. The size of the correction was so small, that continuing the calculations beyond that degree would yield no extra information. Despotakis found the correction term to be 1.5 mm for the OSU86F spherical harmonic reference field. Various reference fields and their corresponding ellipsoidal corrections are given below in Table 15.

TABLE 15

Ellipsoidal corrections using various reference fields. Units in meters

	Model		
Station	OSU86F	OSU89B	OSU91A
7120	0.0015	0.0022	0.0015
7210	0.0015	0.0022	0.0015

For simplicity in later tables, we will apply the ellipsoidal corrections to the outer zone effect in Table 16, and use these values through the rest of the report, remembering that the ellipsoidal corrections are corrections to the complete undulation, not to the outer zone effect.

TABLE 16

Outer zone contribution (meters) to the geoid undulation plus ellipsoidal corrections. Units are meters

		Model					
Ellip.	Sta.	OSU 86 F		OSU 89 B		OSU 91 A	
		180	360	180	360	180	360
OSU87	7120	-1.828	-2.021	-1.033	-1.242	-0.927	-1.137
"	7210	-1.829	-2.021	-1.033	-1.242	-0.927	-1.137
OSU91	7120	-1.828	-2.021	-1.032	-1.242	-0.927	-1.137
"	7210	-1.829	-2.021	-1.033	-1.242	-0.927	-1.137

5.2.6 Undulation from Various Potential Coefficient Models

We have used spherical harmonic reference fields to calculate the outer zone effect on the geoid undulation. It is possible to calculate the entire geoid undulation with only a reference field if the cap size (ψ_C) is set to zero. In this case, no terrestrial gravity data would be required, however, the finite degree of the reference field will introduce errors to the calculated undulation, especially

in areas of high-frequency information (rugged terrain) such as Hawaii.

Despotakis (ibid) calculated an undulation at 7120 and 7210 using the reference field OSU86F up to degree 180. He found a discrepancy between the undulation obtained from physical measurements and the undulation calculated from OSU86F to be near 7.5 meters. This large difference indicates that the limited degree of OSU86F cannot accurately describe the geoid in the rugged area of Maui. Table 17 shows the calculated undulation at 7120 and 7210 using the same three reference fields as used in the previous section, up to degrees 180 and 360. The discrepancies seen in each of these values indicates that we still have a long way to go in producing a finite degree set of harmonic coefficients which can accurately describe rugged areas of the geoid. Note also, that OSU91A appears to be less accurate than OSU89B when compared to the given undulations, assuming the given undulation is correct.

TABLE 17

Geoid undulations calculated by reference fields alone.

Units are meters

			Model					
Ellip.	Sta.	Given N	OSU 86 F		OSU 89 B		OSU 91 A	
			180	360	180	360	180	360
OSU87	7120	20.463	11.854	13.019	14.128	15.905	13.752	15.526
"	7210	20.489	11.858	13.021	14.132	15.907	13.756	15.528
OSU91	7120	20.236	11.855	13.019	14.128	15.905	13.752	15.526
"	7210	20.273	11.858	13.021	14.132	15.907	13.756	15.528

5.2.7 The Entire Geoid Undulation

Using the results in sections 5.2.4 and 5.2.5, many combinations of cap contribution and outer zone contribution can be made. However, it is unreasonable to use old reference fields with new station coordinates, etc. In Tables 18 and 19, the combinations of 3", 30" and 2' TC's with the 3 reference fields are shown. Note that in Tables 12 and 13, the largest effect of assuming changing the crustal density assumption was 0.9 cm. Thus, we will assume $\rho = 2.9 \times 10^3 \text{ kg/m}^3$ for the rest of this report with the understanding that the impact of this assumption is minimal. Also, the difference in effect on the undulation between 30"-1 and 30"-2 TC's is negligible, so we will not differentiate them either. Lastly, the

large difference in OSU89B and OSU91A from OSU86F indicate that these later reference fields are more accurate than their predecessors, which is expected. We shall pair OSU86F and OSU89B with the old system calculations to compare to Despotakis' values, and OSU89B and OSU91A with the new system calculations to show the best current calculation of the geoid undulation at this laser station.

A row of data for values calculated without using terrain corrections is shown as a basis of comparison. These values come strictly from $N_{\Delta g}$, $N_{\delta A}$, Outer zone, and ellipsoidal corrections.

TABLE 18

Geoid Undulation from the Combined Cap, Outer Zone, Indirect Effect,
and Ellipsoidal Corrections, Old system

Station	TC's	OSU86F To 180	OSU86F To 360	OSU89B To 180	OSU89B To 360
7120	No TC's	19.364 m	19.171 m	20.159 m	19.950 m
"	3" - 1	19.379	19.186	20.174	19.965
"	3" - 2	19.363	19.170	20.158	19.949
"	30"	19.497	19.304	20.292	20.083
"	2'	19.409	19.216	20.204	19.995
7210	No TC's	19.362 m	19.170 m	20.158 m	19.949 m
"	3" - 1	19.378	19.186	20.174	19.965
"	3" - 2	19.361	19.169	20.157	19.948
"	30"	19.495	19.303	20.291	20.082
"	2'	19.407	19.215	20.203	19.994

TABLE 19

Geoid Undulation from the Combined Cap, Outer Zone, Indirect Effect,
and Ellipsoidal Corrections, New system

Station	TC's	OSU89B To 180	OSU89B To 360	OSU91A To 180	OSU91A To 360
7120	No TC's	20.182 m	19.972 m	20.287 m	20.077 m
"	3"-1	20.197	19.987	20.302	20.092
"	3"-2	20.181	19.971	20.286	20.076
"	30"	20.315	20.105	20.420	20.210
"	2'	20.227	20.017	20.332	20.122
7210	No TC's	20.180 m	19.971 m	20.286 m	20.076 m
"	3"-1	20.196	19.987	20.302	20.092
"	3"-2	20.179	19.970	20.285	20.075
"	30"	20.313	20.104	20.419	20.209
"	2'	20.225	20.016	20.331	20.121

The difference between the physically measured undulation and the best combinations of calculated undulations for the old system are found in Table 20.

The difference between the physically measured undulation and the best combinations of calculated undulations for the new system are found in Table 21.

TABLE 20

Given undulations minus calculated undulations, Old system.

Units are cm.

Station	TC's	OSU86F To 180	OSU86F To 360	OSU89B To 180	OSU89B To 360
7120	No TC's	109.9	129.2	30.4	51.3
"	3"-1	108.4	127.7	28.9	49.8
"	3"-2	110.0	129.3	30.5	51.4
"	30"	96.6	115.9	17.1	38.0
"	2'	105.4	124.7	25.9	46.8
7210	No TC's	112.7	131.9	33.1	54.0
"	3"-1	111.1	130.3	31.5	52.4
"	3"-2	112.8	132.0	33.2	54.1
"	30"	99.4	118.6	19.8	40.7
"	2'	108.2	127.4	28.6	49.5

TABLE 21

Given undulations minus calculated undulations , New system.

Units are cm.

Station	TC's	OSU89B To 180	OSU89B To 360	OSU91A To 180	OSU91A To 360
7120	No TC's	5.4	26.4	-5.1	15.9
"	3"-1	3.9	24.9	-6.6	14.4
"	3"-2	5.5	26.5	-5.0	16.0
"	30"	-7.9	13.1	-18.4	2.6
"	2'	0.9	21.9	-9.6	11.4
7210	No TC's	9.3	30.2	-1.3	19.7
"	3"-1	7.7	28.6	-2.9	18.1
"	3"-2	9.4	30.3	-1.2	19.8
"	30"	-4.0	16.9	-14.6	6.4
"	2'	4.8	25.7	-5.8	15.2

5.2.8 Discussion of Results

Tables 20 and 21 show that the calculated undulations agree with the given undulations to a range of 17.1 to 132.0 cm in the old system, and -18.4 to 30.3 cm in the new system. Because the computational methods used can have an impact on the undulation at the centimeter level, it is important to understand that any agreement between given and calculated values at a smaller level than 10 cm would not be completely meaningful due to many errors at the cm and mm level which can affect the undulation. Therefore the improvement of reference fields, and gravity data collection will need to be implemented at the same time as better methods of numerical integration, terrain correction calculation and density modelling.

It is alarming to see that when compared to the given undulations, the 3" data has yielded worse results than the 30" data. However, it must first be noted, that we have assumed the given undulations to be free of errors, a poor approximation at best. Realistically, if 3" TC's were calculated accurately, the values of the TC's should yield accurate values of N_{TC} , and N which agree with the true undulations better than the 30" TC's. Because so much care was taken to determine exact TC's at the 3" level, it may be fair to assume that the disagreement between given undulations and calculated undulations (with 3" TC's) is due to error in the given undulations. How and where these errors occur is unknown, but may be because the orthometric height used to calculate the given

undulations was measured from MSL instead of from the geoid. This difference, known as sea surface topography (SST) could easily be in the order of magnitude to correct the disagreement between the given and calculated undulations (with 3" TC's). However, no value for SST that could be known to be consistent, time wise, with the height in this area was known, nor was the particular tide station from which the orthometric heights were measured known. This should be an area of future investigation.

Note, also, that the difference between using terrain corrections on a 3" grid, and not using terrain corrections at all is very small (under 2 cm). This agreement is slightly in error because the border errors were never properly removed from the FFT calculations. Yet, this agreement goes along with a conclusion of Moritz (1968) which we stated earlier, which is that the terrain corrected gravity anomalies may be approximated by the free-air anomalies.

One of the original purposes of this study was to determine why such a large discrepancy occurred in Despotakis (ibid, p. 96) between calculated and given undulations. Table 22 shows the numerical values which Despotakis found in his study.

TABLE 22
Undulation calculations from Despotakis (ibid)

Station	$N_{CAP} = N_{\Delta g} + N_{\delta g_A}$	Outer zone with OSU86F to 360	N_{Total}
7120	20.77	-1.83	18.93
7210	20.80	-1.83	18.96

Note, first, that the cap contribution (N_{CAP}) is immediately in error by 21.6 cm (in 7120) and 18.5 cm (in 7210) due to incorrect referencing of the $\Delta\sigma$ cells in the program used by Despotakis (see section 5.1.1.1).

Because Despotakis used no terrain corrections to his undulations at 7120 and 7210, his N_{CAP} equalled his $N_{\Delta g} + N_{\delta g_A}$. However, we see on Tables 12 and 13 that with the effect of the terrain, the N_{CAP} and $N_{\Delta g} + N_{\delta g_A}$ may differ by as much as 12.1 or 13.1 cm (depending on which ρ is used). As seen on Table 16, the difference between the outer zone effect with OSU86F (to 360) and OSU89B (to 360) is 77.9 cm. Thus, in this case, the effect of using an improved reference field is more than four times that of using terrain corrections on an extremely densified digital terrain model.

Finally, the results of Tables 19 and 21 show the most up-to-date information about the undulation around points 7120 and 7210. Immediately we see that the use of a reference field up to degree 360 does not appear to yield better overall agreement with the given

undulation, yet we do not know that the given undulation is not in error itself.

The questions of which reference field to use, and which crustal density is correct remain. As mentioned, the volcanic nature of the Islands means that the crustal density is somewhere closer to $2.9 \times 10^3 \text{ kg/m}^3$ rather than $2.67 \times 10^3 \text{ kg/m}^3$, however it has been shown that this has an effect less than 1 cm. Lastly, one sees that combining the cap contribution with 30" TC's with the outer zone effect, using OSU91A (to degree 180), gives the best possible agreement with the given undulations. This alone should warrant further study as to why the less dense elevations, and lower degree reference field yield the best agreement with given undulations.

CHAPTER VI

SUMMARY AND CONCLUSIONS

6.1 Summary of Results

Geoid undulations were calculated at two laser station benchmarks (7120, 7210) located on Mt. Haleakala, Maui, Hawaii with corrections being made for the terrain and atmosphere. The method of truncation was used where a cap of radius $\psi_C = 2^\circ$ contained the terrestrial gravity data describing the high frequency information and a spherical harmonic reference field was used to describe the low frequency information outside of that cap. Elevations were available on a 3"x3" grid for most land areas inside of ψ_C and 5'x5' elevations were used to fill in the rest of the elevations. Using the given ellipsoidal coordinates in the SL6 and SL7.1 systems as well as given orthometric heights, the undulations at the laser station were calculated as $N=h-H$ and compared to undulations calculated with truncation theory.

The improvement in using terrain corrections in geoid undulation computations was seen to be dependent upon the grid density of the elevation data available, the method of calculating TC's, and the crustal density assumption. Most influential was the grid density of the available elevation data. The N_{TC} value using 3"

TC's was lower than that using 30" or 2' data by 2.5 to 11.6 cm. Thus, 3" TC's yielded lower undulations than 30" or 2' TC's. These undulations from 3" elevation data disagree with the given undulations by -6.6 to 19.8 cm when used with the OSU91A reference field.

In calculating 3" TC's, a 'border error' occurred, where extraordinarily large TC's were produced from the FFT calculations, along the borders of some 20'x20' calculation areas. This problem could not be resolved, and the large values were simply set to zero.

More important to the geoid undulation was seen to be the improvement of the spherical harmonic reference field used to calculate the outer zone effect. As shown earlier in section 5.2.8, the use of OSU89B over OSU86F changed the outer zone effect on the order of 78 cm, which improved the agreement between given and calculated undulations. The use of OSU91A, however, changed the outer zone effect by 10 cm, but not conclusively improving it. The computation of the geoid undulation through the spherical harmonic reference field alone shows that high frequency information still is not adequately contained in a limited degree reference field -- especially in the Hawaiian Islands, where the terrain changes very rapidly.

The use of a different, possibly more accurate, crustal density assumption was seen to impact the final undulation by less than 1 cm.

The best agreement between given undulations and calculated undulations was under 10 cm, which is within the limits of noise in

these computations, though this did not occur using 3" TC's and OSU91A to degree 360, as would be expected because of their higher accuracy and resolution.

6.2 Conclusions

The agreement between the given and calculated undulations using the 3" TC's is acceptable given the possible noise sources in this study. However, the 3" TC's yielded undulations which disagreed with the given undulations worse than the 30" TC's. Because we have seen that the 3" TC's were very accurately calculated, we assume that some bias exists in the given undulations on the order of 15-20 cm. The source of this bias is unknown, but may be due to sea surface topography (SST). Assuming the given orthometric heights were measured to MSL tide gages, then a correction to the orthometric height should be made for the difference between MSL and the geoid. This difference is SST. No current value is known for the SST value on Maui, nor is the exact tide gage station known, from which the orthometric height was measured.

We have also seen that the use of lengthy, though more computationally accurate, numerical integration programs are not worth the additional computer time. The additional accuracy of under 1cm is considered not worth increasing computer time by many minutes.

For the outer zone effect, the use of any spherical harmonic reference field less accurate than OSU89B will introduce non-negligible errors in the outer zone effect. Also, the use of ellipsoidal corrections is seen to be negligible irregardless of the reference field chosen.

6.3 Areas of Future Research

For the calculation of detailed terrain corrections (with FFT's) to be more accurate, it will be necessary to examine the effect of neglecting elevations outside of the FFT border. This can be done with an FFT program capable of processing 6000 x 6000 points simultaneously, in order to compare TC's to values calculated in small areas and combined into larger files. As stated earlier, the 3"x3" TC's could only be calculated in 20'x20' areas thereby neglecting many elevations in the nearby area.

Also, using a more dense gravity anomaly field may yield more accurate results, as (we assume) the denser TC's did. To improve the $N_{\Delta g}$ values, the use of higher density Δg files directly surrounding the calculation point may yield better results than calculated in this report.

Lastly, the source of the disagreement between the undulation calculated using 3" TC's and the given undulation should be investigated. We have speculated that the SST is the source of this error.

If all these things are done to improve the calculation of the undulation, they may help drive the errors in calculation down to the centimeter level. If this were to happen, some currently accepted computational methods would need to be changed, because we have seen that interpolation of the Stokes' function, numerical integration of the Stokes' integral, accurate crustal densities, and the density of elevation data can have significant effects on the undulation at the centimeter level.

REFERENCES

- Alfano, D., NASA Directory of Station Locations, Flight Dynamics Division, Goddard Space Flight Center, Greenbelt, Maryland, 1986.
- Despotakis, Vasilios K., Geoid Undulation Computations at Laser Tracking Stations, Report No. 383, Dept. of Geodetic Science, The Ohio State University, Columbus, September 1987.
- Engelis, Theodossios, Rapp, Richard H. and Bock, Yehuda, Measuring Orthometric Height Differences with GPS and Gravity Data, manuscripta geodaetica, Vol. 10, pp. 187-194, 1985.
- Forsberg, Rene, A Study of Terrain Reductions, Density Anomalies and Geophysical Inversion Methods in Gravity Field Modelling, Report No. 355, Dept. of Geodetic Science, The Ohio State University, Columbus, April 1984.
- Forsberg, Rene and Sideris, Michael G, Review of Geoid Prediction Methods in Mountainous Regions, Technical Report, Geoid Committee Meeting, Milan, Italy, 1990.
- Goad, Clyde C., Fundamentals of Geodesy, Class Notes, Dept. of Geodetic Science, The Ohio State University, Columbus, 1988.
- Heiskanen, W.H. and Moritz, H., Physical Geodesy, W.H. Freeman and Co., San Francisco, California, 1967.
- Heiskanen, W.A. and Vening Meinesz, F.A., The Earth and Its Gravity Field, McGraw-Hill Book Company, New York, 1958.
- Kim, Jeong-Hee and Rapp, Richard H., Major Dat Sets and Files in the Area of Gravimetric and Altimetric Research, Document, Dept. of Geodetic Science, The Ohio State University, Columbus, August 1990.

- Marsh, J.G. and 16 others, The GEM-T2 Gravitational Model, NASA Technical Memorandum 100746, October 1989.
- Moritz, H., On the Use of the Terrain Correction in Solving Molodensky's Problem, Report No. 108, Dept. of Geodetic Science, The Ohio State University, Columbus, May 1968.
- Moritz, H., Advanced Physical Geodesy, Herbert Wichmann Verlag, Karlsruhe FRG., 1980.
- Pavlis, Erricos C. and Smith, David E., Height Variations of the Global Satellite Laser Tracking Network, 1990 Western Pacific Geophysics Meeting, Kanazawa, Japan, 1990.
- Pavlis, Erricos C., Geodetic and Cartesian Coordinates plus Mean Sea Level Heights, Personal Communication, NASA/Goddard Space Flight Center, 1991.
- Rapp, Richard H and Rummel, R, Methods for the Computation of Detailed Geoids and Their Accuracy, Report No. 233, Dept. of Geodetic Science, The Ohio State University, Columbus, November 1975.
- Rapp, Richard H. and Cruz, J., Spherical Harmonic Expansions of the Earth's Gravitational Potential to Degree 360 Using 30' Mean Anomalies, Report No. 376, Dept. of Geodetic Science, The Ohio State University, Columbus, December 1986.
- Rapp, Richard H. and Nerem, R. Steven and Shum, C.K. and Klosko, Steven M. and Williamson, Ronald G., Consideration of Permanent Tidal Deformation in the Orbit Determination and Data Analysis for the Topex/Poseidon Mission, NASA Technical Memorandum 100775, January 1991.
- Robbins, J.W., and Klosko, S.M., TOPEX Apriori Station Coordinates, Goddard Space Flight Center, Greenbelt, Maryland, 1985.
- Sideris, M.G., A Fast Fourier Transform Method for Computing Terrain Corrections, manuscripta geodaetica, Vol. 10, pp. 66-73, 1985.
- Sloss, Peter W., Digital Relief of the Surface of the Earth, NOAA National Geophysical Data Center, Boulder, Colorado, 1988.

- U.S. Dept. of Defense, Digital Terrain Elevation Data, Defense Mapping Agency, St. Louis, Missouri, 1988.
- Vanicek, P. and Kleusberg, A., The Canadian Geoid - Stokesian Approach, manuscripta geodaetica, Vol. 12, pp. 86-98, 1987.
- Wang, Yan Ming, Downward Continuation of the Free-Air Gravity Anomalies to the Ellipsoid Using the Gradient Solution, Poisson's Integral and Terrain Correction - Numerical Comparison and the Computations, Report No. 393, Dept. of Geodetic Science, The Ohio State University, Columbus, June 1988.
- Wang, Yan Ming and Rapp, Richard H., Terrain effects on geoid undulation computations, manuscripta geodaetica, Vol. 15, pp. 23-29, 1989.
- Wichiencharoen, C., The Indirect Effects on the Computation of Geoid Undulations, Report No. 336, Dept. of Geodetic Science, The Ohio State University, Columbus, December 1982.
- Zhao, Shunde, The Computation of Detailed Geoids Using the Fast Fourier Transform Method, Report No. 400, Dept. of Geodetic Science, The Ohio State University, Columbus, August 1989.